1661-8726/08/020269-20
DOI 10.1007/s00015-008-1260-6
Birkhäuser Verlag, Basel, 2008

Swiss J. Geosci. 101 (2008) 269–288

P-T-t modelling, fluid circulation, and ^{39}Ar-^{40}Ar and Rb-Sr mica ages in the Aar Massif shear zones (Swiss Alps)

Nathalie Challandes [1], Didier Marquer [2,*] & Igor M. Villa [3,4]

Key words: granite, shear zone, ^{39}Ar-^{40}Ar and Rb-Sr ages, fluid circulation, Aar massif, Central Alps

ABSTRACT

Two different 1D forward numerical models of P-T-t paths for the Grimsel granodiorite are evaluated, in order to estimate its retrograde path independently of isotopic ages. The tectonostratigraphic evolution of the External Crystalline Massifs, metamorphic conditions and fluid inclusion data are the essential constraints used to construct these models. Modelled ages are compared with measured ages on micas from the Aar massif, which formed the basis for the controversial "closure temperature" hypothesis. We applied "classical" ^{39}Ar-^{40}Ar and Rb-Sr techniques to two deformation transects in shear zones of the Aar granite and the Grimsel granodiorite. Biotites and white micas crystallised in these shear zones during Miocene deformation under greenschist-facies conditions.

Isotopic ages do not reflect the cooling trajectory calculated by the P-T-t models and cannot be considered as "cooling ages". Instead, K-Ar ages of micas are best viewed as dating local crystallization during ductile greenschist-facies deformation around 21–17 Ma. Whole-rock-mica Rb-Sr ages of ca. 12 Ma demonstrate a chemically open behaviour due to late fluid circulation. The age results indicate that the Rb-Sr record in these rocks, which were deformed under hydrated conditions, provides chronohygrometric information, i.e. on the timing of documented fluid circulation events.

Introduction

This study of mineral ages in shear zones of the External Crystalline Massifs (ECM), Central Swiss Alps, attempts to assess the influence of factors such as deformation, grain size reduction, and fluid circulation on ^{39}Ar-^{40}Ar and Rb-Sr systematics in a regional metamorphic framework. The reported ages are also important in themselves because, as for the whole Alpine chain, there is an ongoing debate regarding the timing of tectonic events in this region (Steck 1984; Dempster 1986; Hunziker et al. 1986; Pfiffner 1986; Burkhard 1988; Kralik et al. 1992; Crespo-Blanc et al. 1995; Kirschner et al. 1995, 1996).

The Aar massif was chosen because there is exceptionally thorough published documentation of its geology, mineralogy, whole-rock and stable isotope geochemistry (Steck 1966, 1968, 1976, 1984; Steck & Burri 1971; Frey et al. 1980; von Raumer 1984; Fourcade et al. 1989; Steck et al. 1989; Marquer & Burkhard 1992; Marquer& Peucat 1994; Schaltegger 1994; Frey & Ferreiro Mählmann 1999; von Raumer et al. 1999). Two ductile shear zones related to Alpine greenschist-facies deformation were selected for this study in two late Variscan granites: the Aar granite and the Grimsel granodiorite (Marquer et al. 1985; Marquer 1990). Neither of these shear zones shows evidence of superimposed structures or hydrothermal alteration associated with late stages of faulting (Kralik et al. 1992; Hofmann et al. 2004).

We have modelled the thermal history of the ECM using a stepwise application of discrete Fourier transform solutions, an alternative to 1-D finite-difference thermal modelling (Mancktelow 1998). The aim of this step is to determine the retrograde path of the ECM independently of any cooling history conventionally inferred from radiogenic dating methods. Then, in two increasingly deformed profiles, we investigated the ^{39}Ar-^{40}Ar and Rb-Sr behaviour in three samples, which show a large grain-size reduction: a weakly deformed rock, an orthogneiss, and a mylonite.

The aim of this study is to compare the isotopic behaviour of these two radiogenic systems with the P-T-t modelling within high-strain deformation zones affecting metagranites. In our samples, grain size reduction is related to increasing strain

[1] Institut de Géologie, 11 Rue Emile Argand, 2007 Neuchâtel, Switzerland.
[2] UMR 6249 Chrono-Environment, Université de Franche-Comté, 16 route de Gray, 25030 Besançon Cedex, France.
[3] Institut für Geologie, Baltzerstrasse 3, 3012 Bern, Switzerland.
[4] Dipartimento di Scienze Geologiche e Geotecnologie, Università di Milano-Bicocca, 20126 Milano, Italy.
*Corresponding author: Didier Marquer. E-mail: didier.marquer@univ-fcomte.fr

intensity. We focused our attention on biotite and white mica ^{39}Ar-^{40}Ar and whole rock-mica Rb-Sr ages because they have been commonly used to constrain the regional "cooling history" of orogenic belts (e.g. Hunziker et al. 1992) or used as indicators of the time of crystallization under greenschist-facies conditions (e.g. Jaeger et al. 1967; Villa 1998; Müller et al. 2000, 2001). A major advantage in this study is that the studied rock types, which were sampled on a small scale (within 10 metres, Aar granite; within 60 metres, Grimsel granodiorite), all experienced the same temperature conditions during the main shearing event. Thus, we can separate the influence of temperature and grain size from other factors such as shear-induced recrystallisation and fluid circulation (Challandes et al. 2003).

Based on ^{39}Ar-^{40}Ar and Rb-Sr mineral dating in these shear zones, we will show that the K-Ar and Rb-Sr systems give evidence for the influence of late fluid circulation. Apparent ages cannot be used to give a "cooling" history and the closure temperature concept does not yield accurate temperature predictions for retrograde metamorphic rocks subject to large fluid circulation, such as those investigated in the Aar massif. Furthermore, the ages provide further constraints on the Oligo-Miocene tectono-metamorphic evolution and the timing of late fluid circulations in the ECM.

Tectono-metamorphic setting

The Aar massif represents a polycyclic basement window exposed within the External Alps of Switzerland (Fig. 1). This ECM belongs to the European plate involved in the Alpine continent-continent collision (Pfiffner et al. 1990a, b) and was thrust towards the northwest under greenschist-facies metamorphic conditions during late Alpine tectonics (Steck 1966,1968, 1984; Choukroune & Gapais 1983; Marquer et al. 1985; Marquer 1987; Pfiffner & Heitzmann 1997). The Aar massif is mainly composed of pre-Variscan gneisses, and Palaeozoic migmatites and amphibolites that were intruded by granites during the late Variscan orogeny (Labhart 1977; Abrecht 1994; Schaltegger 1994).

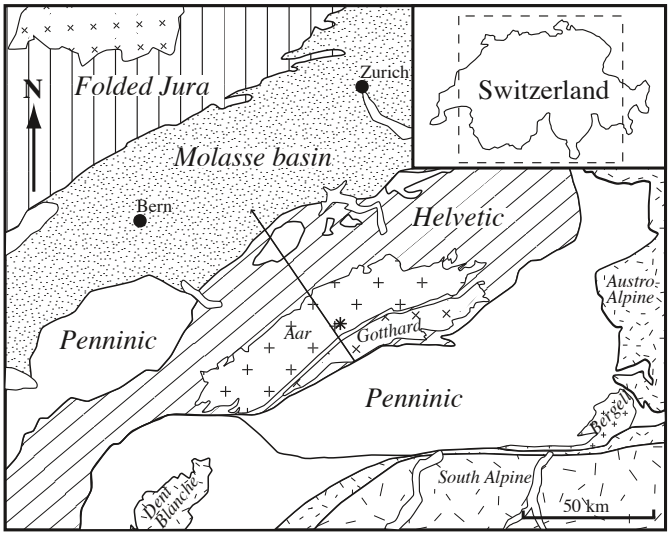

Fig. 1. Simplified geological map of the Swiss Alps. Asterisk in the Aar massif, External Crystalline Massif indicates the location of the studied shear zones (Swiss topographic co-ordinates of samples: Aar granite: 667.90-160.45; Grimsel granodiorite: 668.50-158.40). NW-SE line gives the location of the cross-section on Fig. 3.

The Aar granite and Grimsel granodiorite are part of these Variscan intrusives exposed in the central and southern part of the massif, a few kilometres north of the Grimsel Pass (Stalder 1964). Heterogeneous deformation, during Tertiary NW-SE shortening, formed anastomosing shear zones, which surround lenses of weakly deformed rocks at different scales (Choukroune & Gapais 1983; Marquer et al. 1985; Gapais et al. 1987). The metamorphic conditions associated with this main ductile deformation in the Aar massif show a progressive increase of pressure and temperature from north (300 MPa, 400 °C) to south (400–500 MPa, 450–500 °C) (Steck & Burri 1971; Frey et al. 1974; Steck 1976; Bernotat & Bambauer 1980; Frey et al. 1980; Bambauer & Bernotat 1982; Bernotat & Bambauer 1982; Fourcade et al. 1989). According to the Si-content in phengites, which ranges between 3.2 and 3.3 p.f.u., (Fig. 2a and Tab. 1), and $\delta^{18}O$ analyses of biotite and quartz (Fourcade et al. 1989), the PT conditions of the main shearing event within the Grimsel granodiorite can be estimated at around 450 ± 30 °C and 600 ± 100 MPa (Fig. 2b).

Aar massif shear zones

Both grain size and mineralogy change progressively across the ductile shear zones of the Grimsel granodiorite and Aar granite, leading to syn-kinematic mineral assemblages typical of greenschist-facies conditions. The grain size reduced from an average of 1000 µm in the weakly deformed rocks to around 30 µm in the ultramylonites (Marquer 1987). The Grimsel granodiorite and the Aar granite (alkali felspar, oligoclase, biotite I, quartz) progressively change toward an albite-bearing mylonite (albite, phengite, biotite II, quartz) (see detailed mineralogical descriptions in Marquer 1987). Epidote is stable in the orthogneiss but disappears in the mylonite. The two localities differ in one aspect concerning the Variscan magmatic relics in coarse biotite grains. In the Grimsel granodiorite (Aar 31), biotite is abundant, and the larger grains preserve a magmatic composition (Marquer 1987). In the Aar granite (Aar 10), biotite is rare and more rehomogenized during Tertiary recrystallisation.

The chemical behaviour of radiogenic and stable isotopes, major oxides, and trace and rare earth elements in the Grimsel granodiorite and the Aar granite have been analysed within several metric to hectometric shear zones (Marquer et al. 1985; Marquer 1987; Fourcade et al. 1989; Marquer & Peucat 1994). The geometry of the structures and the geochemical variation profiles across the shear zones are independent of the shear zone size (Marquer 1989). These previous studies mainly documented the enrichment of K, Mg, and Rb and depletion of Na, Ca and Sr in mylonites, while the other element variations

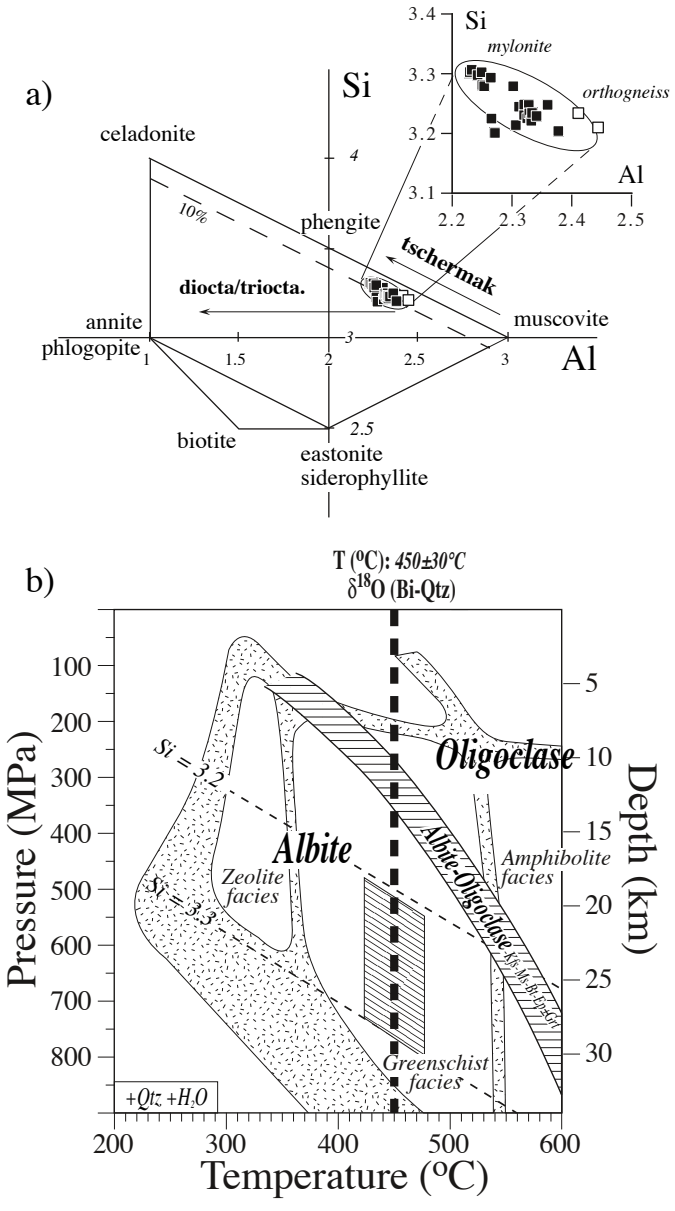

Fig. 2. a) Si/Al-content in phengites in the Grimsel granodiorite shear zone (Table 1). Black squares: mylonites; white squares: orthogneisses. b) P-T conditions of the greenschist-facies deformation affecting the Grimsel granodiorite (oblique stripped area). Temperature conditions: 450 ± 30 °C (Bt-Qtz oxygen isotopes recalculated after Fourcade et al. (1989). Dashed lines corresponding to Si-content in phengites (Fig. 2a) after Massonne and Schreyer (1987). Albite-Oligoclase equilibrium after Maruyama et al. (1983).

remained in the range of initial magmatic variations. The values of whole rock oxygen isotope analyses display an increase in high strain zones (9.65‰) with respect to weakly deformed rocks (7.5‰) (Fourcade et al. 1989). The grain size reduction enhanced the fluid circulation and increased the surface reaction of minerals, improving chemical mass transfer in ductile shear zones (Marquer et al. 1985; Dipple & Ferry 1992). Furthermore, the systematic Rb-Sr variations in the granite and granodiorite shear zones lead to fictitious Early Cretaceous Rb-Sr whole rock ages controlled by partial chemical mass transfer (Marquer & Peucat 1994).

Geological constraints on the age of the main ductile deformation of the ECM

The Alpine schistosity and shear zone patterns of the Aar and Gotthard Massifs were analysed by Choukroune and Gapais (1983) and Marquer (1990). They interpreted the sub-vertical internal structure and stretching in the core of both massifs to be due to a bulk coaxial NW-SE shortening during underthrusting of the ECM. Geometric relationships in the surrounding Helvetic nappes allow superimposed deformations to be distinguished (Milnes & Pfiffner 1980; Burkhard 1988). Burkhard (1988) described five deformation phases (Plaine Morte, Prabé, Trubelstock, Kiental, and Grindelwald phases; Fig. 3) and attributed the steeply dipping ductile schistosity of the internal Aar massif to the Kiental phase (Figs. 3, 4c, 4f). In the southern part of the ECM, this progressive NNW thrusting was followed by backthrusting and SSE-vergent backfolding of the internal units, located south of the Aar massif, contributing to a part of the exhumation of the ECM and to the current large scale structural geometry (Milnes 1976; Voll 1976; Probst 1980; Dolivo, 1982; Steck 1984, 1987; Escher et al. 1997; Steck et al. 1997, 2001). No penetrative deformation related to this younger Grindelwald phase was observed in the studied median part of the Aar massif. Localised slip reactivating the schistosity or discrete thrusting in the ECM could have accommodated late-stage large scale folding in the cover units during the Grindelwald phase.

Considering the non-isotopic age constraints, only the age of incorporation of the Helvetic margin into the accretionary prism is well constrained by biostratigraphy. The Taveyannaz volcano-clastic sandstones were the last sediments to be deposited on the Helvetic Nummulitic platform before burial under the advancing nappe pile (North Helvetic flysch, Fig. 3). The Taveyannaz sandstones are located vertically above the southern part of the Helvetic shelf (Fig.3). They are biostratigraphically correlated with calcareous nannofossils NP21 by Lateltin and Muller (1987) and contain andesitic clasts with Oligocene eruption ages of ca. 33 Ma (Fischer & Villa 1990; Ruffini et al. 1997). They have thus been interpreted to have been deposited between 34.2 and 32.8 Ma (Berggren et al. 1995).

Predicted Pressure-Temperature-time path

The P-T-t paths experienced by rocks involved in mountain building processes depend on many physical and tectonic factors, such as the number and thickness of nappes, erosion and/or tectonic denudation rate. In the literature, P-T-t paths have been numerically derived from several simple tectonic models and, recently, calculated in different thermo-mechanical numerical simulations (England & Richardson 1977; England &

Tab. 1. Electron microprobe analyses of phengites from the Grimsel granodiorite mylonite and orthogneiss*. Mineral formulae are calculated based on 11 oxygens and Fe is assumed divalent.

Label	AD23 phgx-49[1]	AD23 phgx-50[1]	AD23 phgx-51[1]	AD23 phgx-52[1]	AD23 phgx-53[1]	AD23 phgx-54[1]	AD23 phgx-55[1]	AD23 phgx-56[1]	AD23a[2]	ACIIh_1[3]	ACIIh_3[3]	ACIIh_6[3]	ACIIh_6[3]	ACIIh_6[3]
SiO_2	48,54	48,24	48,53	48,37	48,24	48,48	48,33	48,52	48,93	43,27	47,11	45,64	46,43	47,12
TiO_2	0,27	0,32	0,25	0,29	0,26	0,29	0,28	0,29	0,31	0,44	0,37	0,36	0,36	0,26
Al_2O_3	27,80	27,64	27,81	28,20	28,07	27,97	28,20	28,04	29,15	26,05	28,48	28,73	28,24	28,99
FeO*	3,79	3,65	3,84	3,81	3,86	3,57	3,49	3,60	4,03	4,69	3,83	3,66	3,41	3,84
MnO	0,03	0,02	0,02	0,07	0,04	0,03	0,03	0,02	0,02	0,08	0,07	0,10	0,05	0,06
MgO	3,10	2,90	3,01	3,05	3,03	2,93	2,83	2,86	2,65	3,28	2,73	2,62	2,67	2,81
CaO	0,11	0,03	0,02	0,02	0,01	0,00	0,03	0,02	0,00	0,01	0,00	0,06	0,01	0,02
Na_2O	0,12	0,14	0,15	0,12	0,15	0,12	0,13	0,12	0,14	0,15	0,15	0,16	0,17	0,18
K_2O	10,96	11,14	11,34	11,44	11,41	11,55	11,25	11,18	10,68	10,05	11,13	10,68	10,78	10,96
	94,72	94,08	94,97	95,37	95,09	94,94	94,56	94,65	95,91	88,02	93,87	92,01	92,12	94,24
Si	3,30	3,31	3,30	3,28	3,28	3,30	3,29	3,30	3,28	3,20	3,24	3,20	3,25	3,23
Ti	0,01	0,02	0,01	0,01	0,01	0,01	0,01	0,01	0,02	0,02	0,02	0,02	0,02	0,01
Al (tot)	2,23	2,23	2,23	2,25	2,25	2,24	2,26	2,25	2,30	2,27	2,31	2,38	2,33	2,34
Fe^{2+}	0,22	0,21	0,22	0,22	0,22	0,20	0,20	0,20	0,23	0,29	0,22	0,22	0,20	0,22
Mn^{2+}	0,00	0,00	0,00	0,00	0,00	0,00	0,00	0,00	0,00	0,01	0,00	0,01	0,00	0,00
Mg	0,31	0,30	0,31	0,31	0,31	0,30	0,29	0,29	0,27	0,36	0,28	0,27	0,28	0,29
Ca	0,01	0,00	0,00	0,00	0,00	0,00	0,00	0,00	0,00	0,00	0,00	0,00	0,00	0,00
Na	0,02	0,02	0,02	0,02	0,02	0,02	0,02	0,02	0,02	0,02	0,02	0,02	0,02	0,02
K	0,95	0,97	0,98	0,99	0,99	1,00	0,98	0,97	0,91	0,95	0,98	0,96	0,96	0,96
	7,05	7,06	7,07	7,08	7,08	7,08	7,06	7,05	7,02	7,12	7,08	7,08	7,06	7,08
Al^{IV}	0,70	0,69	0,70	0,72	0,72	0,70	0,71	0,70	0,72	0,80	0,76	0,80	0,75	0,77
Al^{VI}	1,53	1,54	1,53	1,53	1,53	1,54	1,56	1,55	1,58	1,47	1,56	1,58	1,58	1,57

[1]thin section, Lausanne 1998. [2]thin section, Marquer 1987. [3]mineral separation, Bern 1999. The AD23 sample is comparable to the ACIIh mylonite sample (Marquer 1987).

Thompson 1984; Davy & Gillet 1986; Karabinos & Ketcham 1988; Ruppel et al. 1988; Ruppel & Hodges 1994; Jamieson et al. 1998; Gerya et al. 2002; Stoeckhert & Gerya 2005). In this work, numerical calculations of P-T-t paths for the Grimsel granodiorite were carried out using a stepwise application of discrete Fourier transform solutions, as implemented in the Macintosh DialogExhume program developed by Mancktelow (1998). For rocks occurring in the Grimsel area, this 1D model was used to establish retrograde P-T-t, P-t and T-t paths for the Grimsel granodiorite (Fig.4). As mentioned in the introduction, it was thought desirable to establish an approximate P-T-t framework for retrograde conditions without resorting to model-dependent interpretations of isotopic behaviour and to circular self-validation of age results.

Initial and boundary conditions

Numerical models for deriving P-T-t paths must start with the mechanisms of thickening: in our case, the under-thrusting of the ECM has led to metamorphic conditions around 600 ± 100 MPa (Fig. 2), corresponding to a depth of about 23 km. Considering a stable continental lithosphere, which is duplicated by "instantaneous thrusting" of one section above another, the resulting geothermal gradient has a saw-tooth shape (Figs. 4a, d, model 1 and 2, respectively; e.g. at 33 Ma). During subsequent thermal relaxation, the shape of the geothermal gradient can be calculated at any time following thrusting (Figs. 4a and d). Several models were tested with different boundary conditions. Here, we present two models where the initial and boundary conditions yield the best fit to the evolution of observed P-T metamorphic conditions in the Grimsel granodiorite (see physical parameters and initial geothermal gradient on Fig. 4).

In both models, the beginning of tectonic burial is placed at 33 Ma, based on the biostratigraphic age of the North Helvetic Taveyannaz sandstones. For simplicity and as assumed in several earlier thematic studies (e.g. England & Thompson, 1984), the prograde burial is formulated as an instantaneous burial to 23 km followed by thermal relaxation without any exhumation. The time following burial needed to reach a temperature of 450 °C is around 10 Ma. Regardless of the simplification in modelling the prograde phase, exhumation after the metamorphic peak conditions (450 °C and 600 MPa) can only begin 10 Ma after sedimentation for any model. From the beginning of exhumation at 23 Ma, the calculated P-T-t path reproduces the temperature increase to a maximum of 450 °C for both models, followed by a decrease in both pressure and temperature. In model 1, the constant exhumation rate is 1 mm/a during the 23 Ma following the P peak, considering mainly denudation by erosion (Figs. 4a, b, and c). In model 2 (Figs. 4d, e, and f), a variable exhumation rate was chosen in order to match zircon and especially apatite fission track data recorded in the Aar massif (Wagner et al. 1977; Michalski & Soom 1990). Model 2 has an exhumation rate of 1 mm/a between 23 and 19 Ma, when

Label	ACIIh_6[3]	ACIIh_6[3]	ACIIh_6[3]	ACIIh_6[3]	ACIIh_6[3]	ACIIh_15[3]	ACIIh_15[3]	ACIIh_2[3]	ACIIh_5[3]	ACIIh_8[3]	ACIId[2]*	AD20[2]*
SiO_2	47,81	47,53	47,26	46,28	46,68	44,05	45,10	46,00	44,67	45,48	47,65	47,67
TiO_2	0,33	0,31	0,30	0,31	0,58	0,39	0,32	0,30	0,36	0,33	0,17	0,22
Al_2O_3	29,13	29,05	28,93	28,05	28,56	27,05	27,80	27,42	27,20	27,94	30,76	30,13
FeO^*	4,13	3,88	3,80	3,54	3,58	4,14	3,21	5,34	4,68	4,61	3,73	3,23
MnO	0,08	0,11	0,00	0,09	0,08	0,04	0,03	0,08	0,06	0,07	0,06	0,05
MgO	2,97	2,82	2,80	2,64	2,72	2,58	2,35	3,24	3,00	2,69	2,15	2,25
CaO	0,04	0,01	0,00	0,00	0,25	0,01	0,01	0,06	0,03	0,04	0,00	0,00
Na_2O	0,12	0,14	0,17	0,16	0,16	0,16	0,16	0,18	0,19	0,16	0,19	0,21
K_2O	11,05	11,16	10,99	10,95	10,88	9,98	10,26	10,70	10,40	10,54	10,57	10,69
	95,66	95,01	94,25	92,02	93,49	88,40	89,24	93,32	90,59	91,86	95,28	94,45
Si	3,23	3,23	3,23	3,25	3,23	3,22	3,25	3,22	3,21	3,22	3,21	3,24
Ti	0,02	0,02	0,02	0,02	0,03	0,02	0,02	0,02	0,02	0,02	0,01	0,01
Al (tot)	2,32	2,33	2,33	2,32	2,33	2,33	2,36	2,27	2,31	2,33	2,44	2,41
Fe^{2+}	0,23	0,22	0,22	0,21	0,21	0,25	0,19	0,28	0,25	0,25	0,21	0,18
Mn^{2+}	0,00	0,01	0,00	0,01	0,01	0,00	0,00	0,01	0,00	0,00	0,00	0,00
Mg	0,30	0,29	0,29	0,28	0,28	0,28	0,25	0,34	0,32	0,28	0,22	0,23
Ca	0,00	0,00	0,00	0,00	0,02	0,00	0,00	0,01	0,00	0,00	0,00	0,00
Na	0,02	0,02	0,02	0,02	0,02	0,02	0,02	0,02	0,03	0,02	0,03	0,03
K	0,95	0,97	0,96	0,98	0,96	0,93	0,94	0,96	0,95	0,95	0,91	0,93
	7,08	7,08	7,07	7,08	7,07	7,07	7,04	7,12	7,10	7,08	7,03	7,03
Al^{IV}	0,77	0,77	0,77	0,75	0,77	0,78	0,75	0,78	0,79	0,78	0,79	0,77
Al^{VI}	1,55	1,56	1,57	1,57	1,55	1,55	1,61	1,49	1,52	1,55	1,65	1,65

peak temperature conditions are reached, 3 mm/a between 19 and 15 Ma, and 0.5 mm/a during the remaining 15 Ma (Fig. 4f). Note that modern estimates for the temperature at which zircon fission tracks are fully annealed is around 330–380 °C (Carpena 1992; Brix et al. 2002; Yamada et al. 2003; Rahn et al. 2004), which is higher than had been assumed by Wagner et al. (1977), although they subsequently also revised their estimate upwards (Coyle & Wagner, 1998). With the mathematical simplification of instantaneous thickening, the P-T-t evolution of the ECM following model 1 was considered because of its simplicity as well as a fair agreement with FT data. In comparison, the results of model 2 involve a rather extreme variation in exhumation rates but give a better fit to the apatite data and to the lowest temperature-time conditions with respect to the zircon data. The P-T-t evolution of the ECM should be bracketed by these two models considering either constant or marked variations of exhumation rate.

Results

Based on the above boundary conditions, P-T-t and P-t–T-t paths of the ECM are drawn in Figs. 4b, e and Figs. 4c, f, respectively. The simplified initial assumption of instantaneous thrusting requires a wait time of 10 Ma in order to achieve the observed P-T maximum of 600 MPa/450 °C. In a more realistic reconstruction, this could be viewed as an average burial/heating rate of 60 MPa/Ma and 45 °C/Ma, respectively. Note that for our purposes the prograde history is not relevant and we therefore can safely use the instantaneous thrusting hypothesis as long as the maximum P-T observations are reproduced. Thus, black and white arrows in Figs. 4b, c, e and f represent the progressive burial of the ECM. In both models, the main shearing event, corresponding to the observed P peak (600 MPa) and T peak (450 °C), is predicted to occur between 23 and 18 Ma (Figs. 4b, e; 4c, f). These results are consistent with the timing of the Kiental phase (Fig. 3: 25–20 Ma according to Burkhard (1988)) and close to the period of Simplon fault activity, located west of the Aar massif (18–15 Ma according to Grasemann & Mancktelow (1993) and Hetherington & Villa (2007)).

Quartz-bearing Alpine fissures also formed as the result of progressive deformation of the ECM (Mullis et al. 1994). These extensional veins are usually subhorizontal and were opened parallel to the vertical stretching lineation. These veins are interpreted as syn- to post-peak temperature and shear zone formation. Thin oblique lines corresponding to fluid inclusion isochores of extensional quartz veins, after Mullis (1996), are drawn on the calculated Oligo-Miocene P-T-t path of the Aar massif (Figs. 4b, e). Intersections of these fluid inclusion isochores with the P–T-t paths give ages of about 18–17 Ma (model 1) or 19–18 Ma (model 2) (high-P intercepts) and between 9 and 5 Ma (model 1) or 14 and 13 Ma (model 2) (low-P intercepts) for the first (a) and the two late generations (b and c), respectively (fluid inclusion

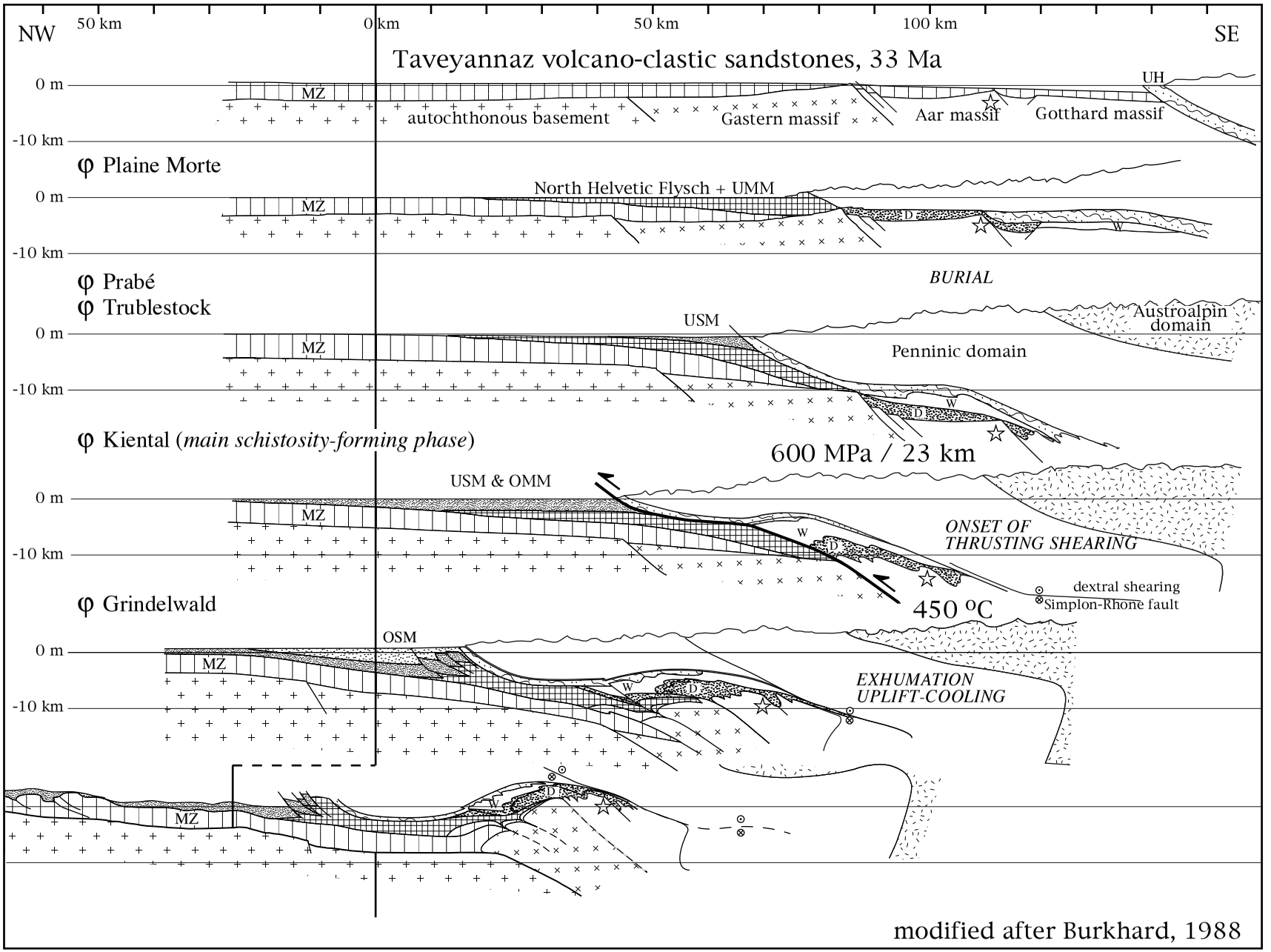

Fig. 3. Tectonic evolution of Alpine front since upper Eocene, modified after Burkhard (1988). White star: projected location of the studied shear zones (Grimsel area, Haslital). MZ: Mesozoic sedimentary cover; UH: Ultra-Helvetic unit; D: Doldenhorn nappe; W: Wildhorn nappe; UMM: Lower Marine Molasse; USM: Lower Fresh Molasse; OMM: Upper Marine Molasse; OSM: Upper Fresh Molasse.

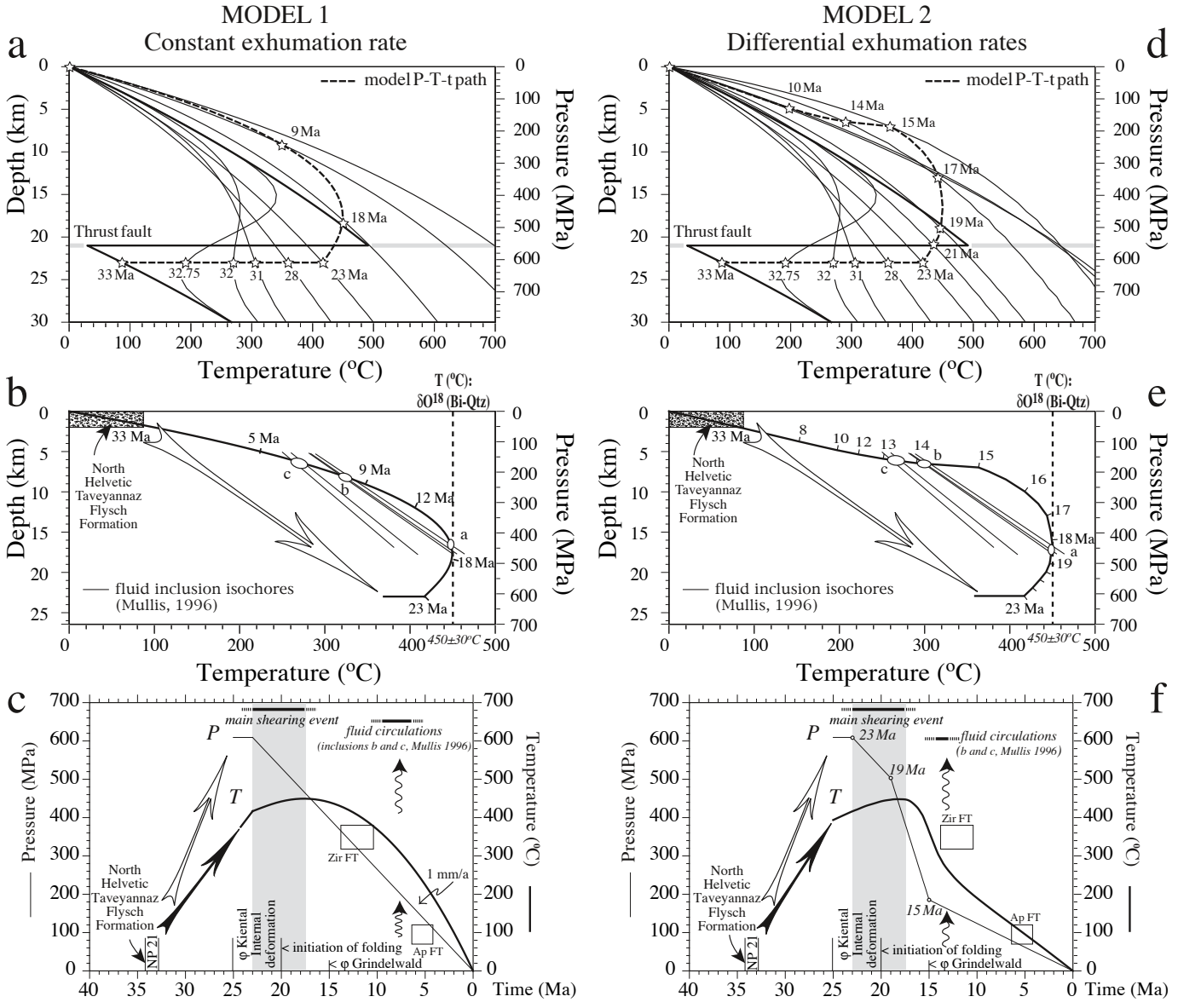

Fig. 4. Two models for the derived P-T-t path of the Grimsel granodiorite (ECM) using a standard discrete Fourier transform solutions (Macintosh DialogExhume program developed by Mancktelow (1998)).

a and d: Modelled time-temperature history. Properties of rocks: thermal diffusivity, 8.42E-07 m^2/sec (Philpotts 1990); surface volumetric heat production, 2.5E-06 W/m^3; heat capacity, 1100 J/kg/K; density, 2700 kg/m^3. The peak pressure of 600 MPa was reached 23 Ma ago; subsequent exhumation histories are: (a) uniform, 1 mm/a; (d) nonuniform, with 1, 3, and 0.5 mm/a, sequentially.

b and e: P-T-t path of the Grimsel granodiorite (ECM) during Oligo-Miocene Alpine tectonics. Vertical dashed line: temperature conditions of the Grimsel granodiorite (cf. Fig.2). Thin oblique lines: fluid inclusions isochores, extensional quartz veins after Mullis (1996).

c and f: Pt–Tt paths of the Grimsel granodiorite (ECM) during Oligo-Miocene Alpine tectonics. Thin line: Pt retrograde modelled path. Bold line: Tt retrograde modelled path. Top of the diagrams: timing of the main shearing event (delay between P and T peaks) and fluid circulation, after fluid inclusion generations b and c (Mullis 1996). Bottom of the diagrams: timing of the Kiental and Grindelwald phases after Burkhard (1988); age of the North Helvetic Taveyannaz Flysch Formation. f: Boxes corresponding to apatite and zircon fission tracks data are from Wagner et al. (1977) and Michalski and Soom (1990).

nomenclature after Mullis et al. 1994). These data are of great importance for the discussion of the geochronological results, because they suggest that late fluid circulation was recorded in the Aar Massif after the main shearing event (generations b and c, Figs. 4c and f).

^{39}Ar-^{40}Ar and Rb-Sr analytical methods

^{39}Ar-^{40}Ar incremental release heating and Rb-Sr techniques were used to investigate five representative samples collected across two deformation gradients (Swiss topographic co-ordinates: Aar granite: 667.90–160.45, Grimsel granodiorite: 668.50

Tab. 2. Argon data of biotites and phengite from the Aar granite.

Step	Temp. (°C)	^{39}Ar %	^{40}Ar total (ml)	1σ (abs.) (ml)	^{40}Ar* (ml)	^{39}Ar (ml)	1σ (abs.) (ml)	^{38}Ar (ml)	1σ (abs.) (ml)	^{38}Ar Cl (ml)	^{37}Ar (ml)	1σ (abs.) (ml)
Sample Aar10 (*grain size: 1000 µm*): Weakly deformed rock – biotite (J = 0.00414, mass = 11.25 mg)												
1	652	4,5	7,05E-09	±8,10E-12	2,70E-09	8,16E-10	±1,10E-12	1,65E-11	±1,60E-13	4,22E-12	1,74E-10	±2,00E-12
2	704	7,1	4,02E-09	±2,20E-12	2,95E-09	1,28E-09	±2,30E-12	2,22E-11	±2,80E-13	6,42E-12	1,43E-10	±1,73E-12
3	749	10,0	5,32E-09	±6,90E-12	4,29E-09	1,82E-09	±2,50E-12	2,75E-11	±1,90E-13	5,46E-12	1,66E-10	±2,09E-12
4	802	17,2	8,33E-09	±2,40E-11	7,46E-09	3,12E-09	±9,40E-12	4,89E-11	±2,50E-13	1,16E-11	2,16E-10	±2,97E-12
5	853	10,7	5,59E-09	±2,80E-11	4,61E-09	1,94E-09	±10,00E-12	2,72E-11	±2,50E-13	3,79E-12	9,68E-11	±2,91E-12
6	900	5,1	3,05E-09	±2,30E-11	2,02E-09	9,27E-10	±4,70E-12	1,61E-11	±2,20E-13	4,57E-12	7,69E-11	±1,81E-12
7	966	6,3	3,94E-09	±10,00E-13	2,78E-09	1,14E-09	±10,00E-13	1,91E-11	±1,90E-13	5,04E-12	4,78E-10	±1,65E-12
8	1028	10,5	5,63E-09	±1,80E-12	4,65E-09	1,91E-09	±2,00E-12	2,94E-11	±7,60E-14	6,43E-12	7,26E-10	±2,86E-12
9	1087	12,7	6,47E-09	±3,10E-12	5,86E-09	2,31E-09	±2,40E-12	3,57E-11	±2,00E-13	8,25E-12	4,65E-10	±2,31E-12
10	1140	9,2	4,84E-09	±3,10E-12	3,95E-09	1,66E-09	±2,10E-12	2,53E-11	±2,00E-13	5,32E-12	8,56E-10	±3,49E-12
11	1190	4,8	3,24E-09	±4,40E-13	2,22E-09	8,76E-10	±8,00E-13	1,43E-11	±1,50E-13	3,65E-12	2,20E-09	±6,56E-12
12	1266	1,3	1,41E-09	±1,60E-12	8,26E-10	2,27E-10	±2,80E-13	4,48E-12	±2,30E-13	1,81E-12	2,66E-09	±8,23E-12
13	1499	0,5	1,14E-09	±1,20E-12	8,04E-11	9,45E-11	±2,60E-13	1,89E-12	±1,20E-13	3,59E-13	1,74E-09	±7,00E-12
Step	**Temp. (°C)**	**^{39}Ar %**	**^{40}Ar total (ml)**	**1σ (abs.) (ml)**	**^{40}Ar* (ml)**	**^{39}Ar (ml)**	**1σ (abs.) (ml)**	**^{38}Ar (ml)**	**1σ (abs.) (ml)**	**^{38}Ar Cl (ml)**	**^{37}Ar (ml)**	**1σ (abs.) (ml)**
Sample Aar17 (*grain size: 30 µm*): Mylonitic rock – biotite (J = 0.00657, mass = 11.3 mg)												
1	451	4,5	2,08E-08	±1,40E-12	1,45E-09	3,16E-10	±3,20E-13	2,01E-11	±2,10E-13	4,18E-12	7,37E-12	±3,48E-12
2	498	5,3	1,15E-08	±9,80E-13	4,84E-10	3,78E-10	±3,80E-13	1,36E-11	±1,50E-13	2,19E-12	1,99E-11	±3,02E-12
3	545	7,7	7,40E-09	±5,00E-13	9,09E-10	5,47E-10	±5,20E-13	1,26E-11	±2,00E-13	2,04E-12	8,47E-12	±2,73E-12
4	574	6,6	4,07E-09	±1,40E-12	5,95E-10	4,69E-10	±4,90E-13	1,09E-11	±7,90E-14	3,15E-12	2,61E-11	±3,05E-12
5	601	5,7	8,14E-09	±6,10E-13	8,23E-10	4,02E-10	±4,40E-13	1,36E-11	±3,00E-13	4,21E-12	1,72E-11	±4,02E-12
6	659	19,1	5,36E-09	±5,30E-13	2,71E-09	1,35E-09	±1,20E-12	2,17E-11	±2,60E-13	4,16E-12	1,75E-11	±3,43E-12
7	712	23,9	5,22E-09	±7,00E-13	2,75E-09	1,69E-09	±1,50E-12	2,78E-11	±2,60E-13	6,43E-12	8,12E-11	±4,39E-12
8	764	10,3	3,47E-09	±3,90E-13	1,25E-09	7,27E-10	±7,00E-13	1,30E-11	±2,30E-13	3,02E-12	6,50E-11	±1,85E-12
9	838	4,9	4,19E-09	±4,90E-13	5,44E-10	3,46E-10	±3,90E-13	7,16E-12	±1,80E-13	7,80E-13	4,28E-11	±3,64E-12
10	884	3,2	3,58E-09	±4,40E-13	7,05E-10	2,29E-10	±3,00E-13	5,85E-12	±2,20E-13	1,35E-12	6,43E-11	±4,11E-12
11	925	1,6	2,39E-09	±7,70E-14	2,93E-10	1,10E-10	±1,70E-13	2,98E-12	±1,20E-13	3,62E-13	3,33E-11	±8,80E-13
12	969	1,2	2,06E-09	±4,20E-13	2,32E-10	8,67E-11	±1,70E-13	1,47E-12	±2,20E-13	–6,89E-13	6,55E-11	±4,76E-12
13	1026	1,0	2,50E-09	±5,20E-13	2,01E-10	7,11E-11	±1,80E-13	2,26E-12	±2,10E-13	–1,28E-14	7,48E-11	±4,26E-12
14-new	1402	5,0	3,56E-08	±1,51E-11	1,395E-09	3,51E-10	±4,04E-13	2,795E-11	±3,07E-13	0,0	2,78E-10	±5,83E-12
Step	**Temp. (°C)**	**^{39}Ar %**	**^{40}Ar total (ml)**	**1σ (abs.) (ml)**	**^{40}Ar* (ml)**	**^{39}Ar (ml)**	**1σ (abs.) (ml)**	**^{38}Ar (ml)**	**1σ (abs.) (ml)**	**^{38}Ar Cl (ml)**	**^{37}Ar (ml)**	**1σ (abs.) (ml)**
Sample Aar17 (*grain size: 30 µm*): Mylonitic rock – phengite (J = 0.00414, mass = 6.47 mg)												
1	440	3,3	2,09E-08	±1,30E-11	8,80E-10	2,59E-10	±3,50E-13	2,38E-11	±2,90E-13	8,14E-12	2,38E-11	±4,27E-12
2	488	4,3	4,26E-09	±9,30E-13	8,83E-10	3,43E-10	±3,90E-13	1,26E-11	±2,50E-13	6,48E-12	2,93E-11	±5,14E-12
3	537	7,1	3,31E-09	±2,10E-12	1,47E-09	5,62E-10	±5,90E-13	1,28E-11	±2,80E-13	5,00E-12	2,70E-11	±5,62E-12
4	567	9,2	3,05E-09	±1,80E-12	1,50E-09	7,35E-10	±7,20E-13	1,25E-11	±1,80E-13	2,90E-12	3,93E-11	±3,53E-12
5	597	8,4	3,09E-09	±1,50E-12	1,59E-09	6,69E-10	±6,40E-13	1,14E-11	±2,20E-13	2,54E-12	3,20E-11	±3,14E-12
6	652	10,4	3,09E-09	±1,10E-12	1,79E-09	8,30E-10	±7,50E-13	1,40E-11	±1,80E-13	3,42E-12	2,33E-11	±5,40E-12
7	706	8,8	2,77E-09	±6,70E-13	1,39E-09	7,02E-10	±6,50E-13	1,14E-11	±1,30E-13	2,27E-12	3,64E-11	±3,86E-12
8	754	8,9	2,79E-09	±8,70E-13	1,46E-09	7,07E-10	±6,70E-13	1,11E-11	±1,40E-13	1,97E-12	3,75E-11	±3,01E-12
9	829	13,4	3,71E-09	±1,20E-12	2,35E-09	1,07E-09	±9,70E-13	1,63E-11	±2,10E-13	2,88E-12	4,21E-11	±5,35E-12
10	898	15,3	4,17E-09	±1,10E-12	2,96E-09	1,22E-09	±1,10E-12	1,91E-11	±3,10E-13	4,06E-12	4,57E-11	±2,73E-12
11	963	6,3	2,33E-09	±5,60E-13	1,39E-09	5,04E-10	±5,20E-13	7,72E-12	±7,80E-14	1,21E-12	3,88E-11	±4,79E-12
12	1021	2,2	1,37E-09	±2,80E-13	2,91E-10	1,72E-10	±1,90E-13	4,60E-12	±1,80E-13	1,91E-12	5,54E-11	±3,69E-12
13	1074	1,2	1,05E-09	±3,00E-13	–8,71E-11	9,29E-11	±2,60E-13	3,53E-12	±1,90E-13	1,72E-12	6,72E-11	±3,90E-12
14	1159	1,0	1,22E-09	±1,70E-13	1,671E-10	8,28E-11	±1,10E-13	6,045E-12	±2,80E-13	0,0	9,30E-11	±2,15E-12

–158.40), from weakly deformed granites (Aar10 and Aar 31) to orthogneisses (AD20) and mylonites (Aar17 and ACIIh). These samples provided seven multi-grain mineral separates (five biotites, two phengites). In addition to these samples, three mica analyses and one whole rock analysis from Marquer (1987) are included in the present discussion (Table 4).

Mineral separation

Samples were crushed and sieved. Visual inspection of the coarser fractions showed that multi-grain aggregates were a major problem, especially for mylonitic samples whose natural grain size is lower than 30 µm. Therefore, the 10 µm–50 µm

^{36}Ar (ml)	1σ (abs.) (ml)	Cl/K	1σ (abs.)	Ca/K	1σ (abs.)	Age (Ma)	1σ (abs.) (Ma)	^{39}Ar/^{40}Ar	1σ (abs.)	^{36}Ar/^{40}Ar	1σ (abs.)
1,47E-11	±2,20E-13	1,19E-03	±4,67E-05	4,26E-01	±4,90E-03	24,6	±0,6	1,16E-01	±2,10E-04	2,09E-03	±3,20E-05
3,69E-12	±2,00E-13	1,15E-03	±5,09E-05	2,22E-01	±2,70E-03	17,1	±0,3	3,19E-01	±6,00E-04	9,07E-04	±5,00E-05
3,51E-12	±2,00E-13	6,90E-04	±2,48E-05	1,83E-01	±2,30E-03	17,5	±0,2	3,42E-01	±6,40E-04	6,52E-04	±3,70E-05
3,00E-12	±1,90E-13	8,57E-04	±2,03E-05	1,38E-01	±1,90E-03	17,8	±0,2	3,75E-01	±1,60E-03	3,54E-04	±2,20E-05
3,34E-12	±2,00E-13	4,51E-04	±3,31E-05	10,00E-02	±3,00E-03	17,7	±0,3	3,47E-01	±2,50E-03	5,93E-04	±3,50E-05
3,50E-12	±1,80E-13	1,13E-03	±5,69E-05	1,66E-01	±3,90E-03	16,2	±0,5	3,03E-01	±2,80E-03	1,14E-03	±6,10E-05
4,05E-12	±1,90E-13	1,02E-03	±3,92E-05	8,42E-01	±2,90E-03	18,2	±0,4	2,88E-01	±2,70E-04	9,96E-04	±4,60E-05
3,51E-12	±1,80E-13	7,76E-04	±1,04E-05	7,62E-01	±3,00E-03	18,1	±0,2	3,38E-01	±3,70E-04	5,91E-04	±3,10E-05
2,19E-12	±1,90E-13	8,21E-04	±2,04E-05	4,03E-01	±2,00E-03	18,9	±0,2	3,57E-01	±4,10E-04	3,20E-04	±2,80E-05
3,23E-12	±2,00E-13	7,35E-04	±2,83E-05	1,03E+00	±4,20E-03	17,6	±0,2	3,44E-01	±4,80E-04	6,22E-04	±3,80E-05
4,01E-12	±1,80E-13	9,58E-04	±4,04E-05	5,03E+00	±1,50E-02	18,9	±0,4	2,70E-01	±2,50E-04	1,06E-03	±4,70E-05
2,67E-12	±2,00E-13	1,83E-03	±2,36E-04	2,36E+01	±7,30E-02	27,1	±1,4	1,60E-01	±2,60E-04	1,41E-03	±1,00E-04
4,03E-12	±2,10E-13	8,74E-04	±3,07E-04	3,72E+01	±1,50E-01	6,4	±4,3	8,19E-02	±2,40E-04	3,15E-03	±1,60E-04
^{36}Ar (ml)	**1σ (abs.) (ml)**	**Cl/K**	**1σ (abs.)**	**Ca/K**	**1σ (abs.)**	**Age (Ma)**	**1σ (abs.) (Ma)**	**^{39}Ar/^{40}Ar**	**1σ (abs.)**	**^{36}Ar/^{40}Ar**	**1σ (abs.)**
6,53E-11	±3,40E-13	3,04E-03	±1,60E-04	4,66E-02	±2,20E-02	53,6	±3,7	1,52E-02	±1,50E-05	3,15E-03	±1,60E-05
3,74E-11	±2,30E-13	1,33E-03	±9,50E-05	1,05E-01	±1,60E-02	15,1	±2,1	3,28E-02	±3,30E-05	3,24E-03	±2,00E-05
2,20E-11	±1,70E-13	8,57E-04	±8,52E-05	3,01E-02	±1,00E-02	19,6	±1,1	7,38E-02	±7,00E-05	2,97E-03	±2,30E-05
1,18E-11	±1,30E-13	1,54E-03	±4,07E-05	1,12E-01	±1,30E-02	15,0	±1,0	1,15E-01	±1,30E-04	2,89E-03	±3,20E-05
2,48E-11	±1,50E-13	2,40E-03	±1,72E-04	8,54E-02	±2,00E-02	24,1	±1,3	4,95E-02	±5,40E-05	3,04E-03	±1,80E-05
8,96E-12	±1,80E-13	7,11E-04	±4,49E-05	2,60E-02	±5,10E-03	23,7	±0,5	2,51E-01	±2,30E-04	1,67E-03	±3,30E-05
8,39E-12	±1,40E-13	8,76E-04	±3,57E-05	9,62E-02	±5,20E-03	19,2	±0,3	3,23E-01	±2,90E-04	1,60E-03	±2,60E-05
7,54E-12	±1,60E-13	9,53E-04	±7,34E-05	1,79E-01	±5,10E-03	20,3	±0,8	2,09E-01	±2,00E-04	2,17E-03	±4,60E-05
1,23E-11	±1,20E-13	5,17E-04	±1,20E-04	2,47E-01	±2,10E-02	18,5	±1,2	8,27E-02	±9,40E-05	2,94E-03	±2,90E-05
9,75E-12	±2,10E-13	1,36E-03	±2,25E-04	5,63E-01	±3,60E-02	36,2	±3,2	6,38E-02	±8,50E-05	2,72E-03	±6,00E-05
7,12E-12	±1,10E-13	7,58E-04	±2,55E-04	6,05E-01	±1,60E-02	31,3	±3,6	4,60E-02	±7,20E-05	2,97E-03	±4,80E-05
6,19E-12	±1,40E-13	–1,83E-03	±5,88E-04	1,51E+00	±1,10E-01	31,5	±5,7	4,21E-02	±8,10E-05	3,00E-03	±6,90E-05
7,77E-12	±1,70E-13	–4,13E-05	±6,87E-04	2,11E+00	±1,20E-01	34,6	±8,3	2,84E-02	±7,10E-05	3,10E-03	±6,90E-05
1,159E-10	±4,95E-13	1,46E-03	±2,10E-04	1,59E+00	±3,33E-02	46,5	±4,9	9,85E-03	1,21E-05	3,25E-03	1,39E-05
^{36}Ar (ml)	**1σ (abs.) (ml)**	**Cl/K**	**1σ (abs.)**	**Ca/K**	**1σ (abs.)**	**Age (Ma)**	**1σ (abs.) (Ma)**	**^{39}Ar/^{40}Ar**	**1σ (abs.)**	**^{36}Ar/^{40}Ar**	**1σ (abs.)**
6,77E-11	±4,50E-13	7,23E-03	±2,68E-04	1,84E-01	±3,30E-02	25,2	±3,8	1,24E-02	1,80E-05	3,24E-03	2,20E-05
1,14E-11	±4,60E-13	4,35E-03	±1,77E-04	1,71E-01	±3,00E-02	19,1	±2,9	8,04E-02	9,40E-05	2,68E-03	1,10E-04
6,22E-12	±4,00E-13	2,05E-03	±1,19E-04	9,63E-02	±2,00E-02	19,4	±1,5	1,70E-01	2,10E-04	1,88E-03	1,20E-04
5,22E-12	±3,90E-13	9,09E-04	±6,09E-05	1,07E-01	±9,60E-03	15,2	±1,2	2,41E-01	2,80E-04	1,71E-03	1,30E-04
5,11E-12	±3,90E-13	8,72E-04	±7,97E-05	9,57E-02	±9,40E-03	17,6	±1,3	2,16E-01	2,30E-04	1,65E-03	1,30E-04
4,42E-12	±3,80E-13	9,49E-04	±5,37E-05	5,61E-02	±1,30E-02	16,0	±1,0	2,68E-01	2,60E-04	1,43E-03	1,20E-04
4,66E-12	±4,10E-13	7,43E-04	±4,95E-05	1,04E-01	±1,10E-02	14,7	±1,3	2,54E-01	2,40E-04	1,68E-03	1,50E-04
4,49E-12	±3,90E-13	6,41E-04	±5,14E-05	1,06E-01	±8,50E-03	15,4	±1,2	2,54E-01	2,50E-04	1,61E-03	1,40E-04
4,62E-12	±3,90E-13	6,19E-04	±4,79E-05	7,88E-02	±1,00E-02	16,4	±0,8	2,88E-01	2,80E-04	1,24E-03	1,00E-04
4,09E-12	±4,30E-13	7,69E-04	±6,07E-05	7,52E-02	±4,50E-03	18,1	±0,8	2,91E-01	2,70E-04	9,78E-04	1,00E-04
3,17E-12	±4,60E-13	5,50E-04	±5,30E-05	1,54E-01	±1,90E-02	20,5	±2,0	2,17E-01	2,30E-04	1,36E-03	1,90E-04
3,68E-12	±3,90E-13	2,55E-03	±2,60E-04	6,46E-01	±4,30E-02	12,6	±4,9	1,25E-01	1,40E-04	2,67E-03	2,80E-04
3,87E-12	±4,30E-13	4,26E-03	±5,11E-04	1,45E+00	±8,40E-02	–7,0	±–10,0	8,84E-02	2,40E-04	3,66E-03	4,00E-04
3,593E-12	±4,10E-13	1,23E-02	±8,06E-04	2,25E+00	±5,20E-02	15,0	±11,0	6,78E-02	8,80E-05	2,92E-03	3,30E-04

fraction was obtained by sedimentation in Attenberg cylinders. Magnetic separation allowed the separation of biotite from phengite. However, density separation failed due to the poor wetting and high clustering of grains. Thus, all separates contained significant amounts of quartz ± plagioclase, particularly in granite mylonite samples.

^{39}Ar-^{40}Ar techniques

Mineral concentrates, biotites, and phengites were analysed using incremental-heating ^{39}Ar-^{40}Ar analysis, following techniques described in detail by Belluso et al. (2000). Incremental heating techniques provide a quality filter for the data based

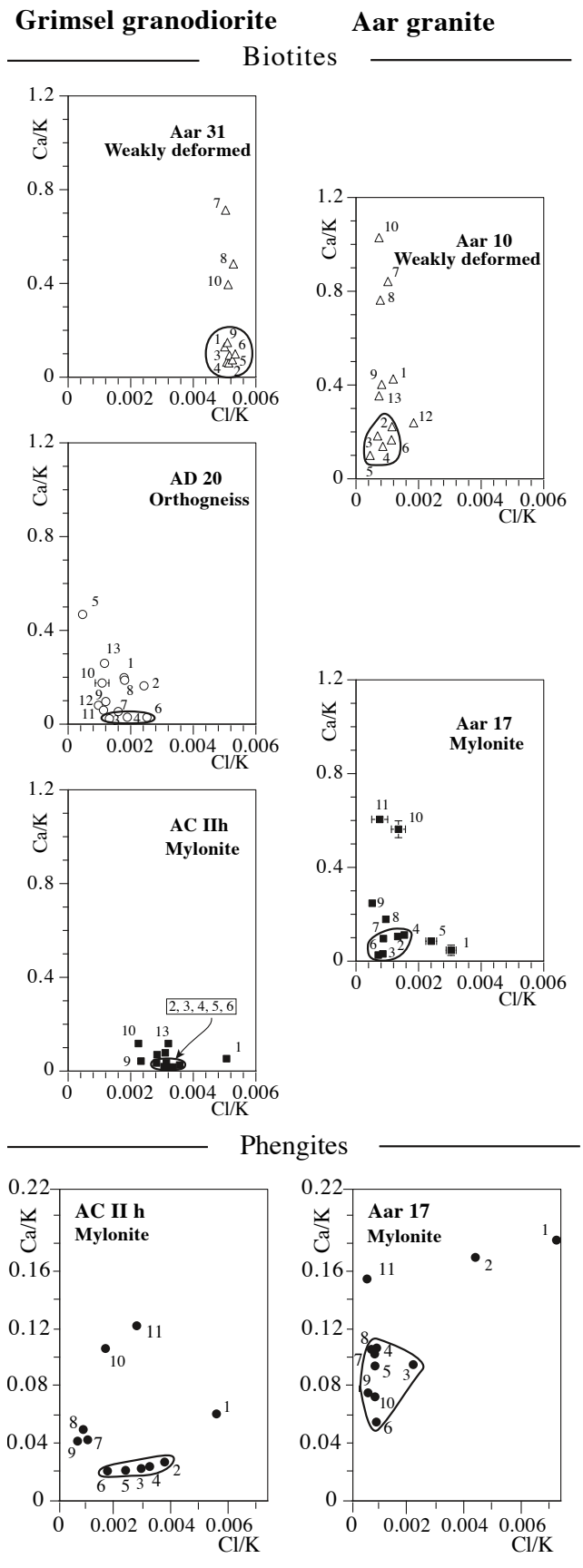

Fig. 5. a and b: Ca-Cl-K correlation diagram for biotites and phengites of the Aar granite and Grimsel granodiorite (note Ca/K scale change for phengites). Biotites: open triangles: weakly deformed rocks; open dots: orthogneisses; black squares: mylonites. Phengites: black dots. Error bars are smaller than symbol size except where shown. Surrounded areas correspond to steps used to calculate isochemical ages (Fig. 6).

on chemical signatures. ^{37}Ar, ^{38}Ar, and ^{39}Ar isotopes are produced by several reactions caused by interactions of neutrons with the isotopes of calcium, chlorine, and potassium during irradiation (Brereton 1970). Thus, these three Ar isotopes provide substantial chemical information that can be used to discriminate different phases. Complex ^{39}Ar-^{40}Ar age spectra are interpreted using the systematics defined for mineral mixtures (Belluso et al. 2000; Villa et al. 2000; Müller et al. 2002). Chemical information provided by the Ca-Cl-K correlation diagrams (Fig. 5) were taken into account to estimate ^{39}Ar-^{40}Ar ages of biotite and white mica from the "isochemical" steps (i.e. those steps with homogeneous Ca/K and Cl/K ratios as determined from the argon isotopes, $^{39}Ar_K$, $^{38}Ar_{Cl}$, $^{37}Ar_{Ca}$). The validation of the chemical discrimination approach is provided by Villa et al. (2000). Note that the chronologically relevant steps of a mixture need not encompass a very large part of the Ar release (Villa et al. 2000, Müller et al. 2002). What is more important is the Ca-Cl-K signature of the pure end-members of the mixture. The drawback of the quartz ± plagioclase impurities (clearly visible from the high Ca/K ratios (Fig. 5)) is that they make it impossible to use the sub-stoichiometric K concentrations as a monitor of chloritization. The Ar isotope systematics of chloritization are addressed by Di Vincenzo et al. (2003). Finally, we note that from a chronometric point of view the importance of the present impurity phases is subordinate. The inter-sample age variations (17–21 Ma) are larger than the within-sample bias that can be produced by adding or removing one more step to the isochemical set. The ^{39}Ar-^{40}Ar analytical data are listed in Tables 2 and 3 with 1-sigma errors and are depicted as age spectra in Fig. 6.

Rb-Sr techniques

Rb and Sr concentrations were determined by isotope dilution, using a mixed ^{87}Rb-^{84}Sr spike. Rb was measured on an AVCO™ single-collector thermal ionisation mass spectrometer and Sr on a VG 354 multicollector thermal ionisation mass spectrometer, both in Bern. Analytical details of Rb and Sr analyses performed at the University of Rennes are described in Marquer (1987) and Marquer and Peucat (1994). Rb/Sr whole rock-mineral ages are calculated with the Isoplot/Ex program, version 2.2 (Ludwig 2000). Age results, calculated with the decay constant $\lambda = 1.42\ 10^{-11}\ a^{-1}$ and 2-sigma errors, are given in Table 4.

Geochronological results

^{39}Ar-^{40}Ar data

As seen in Fig. 6, none of the seven ^{39}Ar-^{40}Ar age spectra for biotites and phengites from the Aar granite and Grimsel granodiorite samples shows a simple plateau. Generally, the low and high-temperature steps give a disturbed pattern. Integrated ages are calculated on the total steps.

Isochemical ages are defined by using a chemical correlation diagram (Fig. 5), following the diagnostic approach of Belluso et al. (2000) and Villa et al. (2000). As shown by these authors, complex ^{39}Ar-^{40}Ar age spectra that give no plateau can be successfully interpreted, provided that the sample mineralogy and microchemistry can be tied to discordant features of the age spectra and end-member components in 3-isotope correlation plots. The chemical correlation diagrams of biotites and phengites analysed in the Aar granite and Grimsel granodiorite shear zones are shown in Fig. 5. For every sample in these diagrams, many points cluster near low Ca/K and low Cl/K end-members. We interpret these clusters as closest to the true biotite and phengite compositions and therefore only the lowest Ca/K steps are used to calculate the isochemical ages (Tables 2–3 and Fig. 6).

Biotite Aar 31 (Fig. 6) yields an age of 37.1 ± 0.8 Ma, intermediate between Variscan magmatism and the deformation age indicated by all other samples. In view of the petrographic observation mentioned above, the presence of magmatic biotite relics is the probable cause of isotopic inheritance (cf. Villa 1998). Except for this sample, all integrated and isochemical mica age estimates are between 23 and 16 Ma and 21 and 17 Ma, respectively. Because the integrated K-Ar (total-gas) ages obviously mix steps corresponding to different chemical compositions, these are not the same as the isochemical ages (Fig. 6) and have no geological meaning. However, the difference between the total-gas and the isochemical ages is never very large, being + 3.3 Ma in only one instance and + 0.2 Ma on average.

^{39}Ar-^{40}Ar interpretation

In Dodson's (1973) approach, the closure temperature (T_c) of a geochronological system is defined as its temperature at the time corresponding to its isotopic age. This assumption is only valid if the mineral grew above this closure temperature. Isotopic diffusion is then assumed to be negligible below the closure temperature. Based on the parameters of volume diffusion, a closure temperature can be calculated (Dodson 1973). K-Ar biotite closure temperatures can be calculated for the three sampled rocks, using diffusion coefficient and activation energy of 0.78 cm^2/s and 250 kJ/mol, respectively (Villa & Puxeddu 1994), and assuming a cylindrical geometry. The average grain sizes are 1000 μm in weakly deformed rocks, 300 μm in orthogneiss and 30 μm in mylonites (Fig. 7). For average cooling rates of 10 and 40 °C/Ma, corresponding to numerical models 1 and 2, the calculated closure temperatures are 489, 445, and 374, and 517, 470, and 394 °C, respectively. Projecting these values onto the modelled T-t paths predicts a substantial decrease in the biotite cooling ages with reduction of the grain

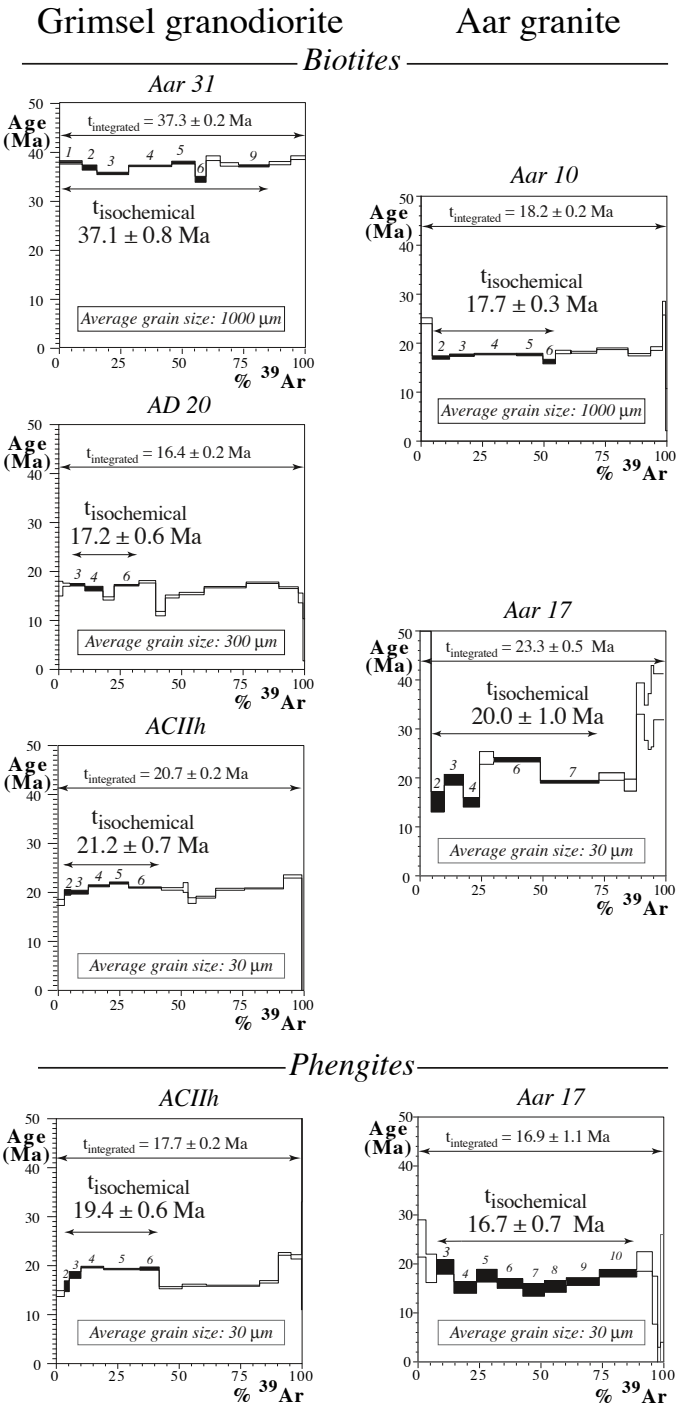

Fig. 6. Biotite and phengite ^{39}Ar-^{40}Ar age spectra for the Aar granite and Grimsel granodiorite samples. Integrated ages are performed on the total steps. Isochemical ages are highlighted in black and were defined as the low-Ca steps in the chemical correlation diagrams of Fig. 5.

Tab. 3. Argon data of biotites and phengite from the Grimsel granodiorite.

Step	Temp. (°C)	^{39}Ar %	^{40}Ar total (ml)	1σ (abs.) (ml)	^{40}Ar* (ml)	^{39}Ar (ml)	1σ (abs.) (ml)	^{38}Ar (ml)	1σ (abs.) (ml)	^{38}Ar Cl (ml)	^{37}Ar (ml)	1σ (abs.) (ml)
Sample Aar31 (*grain size: 1000 μm*): Weakly deformed rock – biotite (J = 0.00414, mass = 10.11 mg)												
1	650	9,3	1,05E-08	±3,20E-12	7,82E-09	1,52E-09	±1,50E-12	5,27E-11	±1,90E-13	3,31E-11	9,86E-11	±3,96E-12
2	740	6,0	5,16E-09	±1,30E-12	4,89E-09	9,80E-10	±9,40E-13	3,35E-11	±2,10E-13	2,18E-11	3,15E-11	±5,88E-12
3	793	12,9	1,12E-08	±10,00E-12	1,02E-08	2,11E-09	±2,90E-12	7,29E-11	±2,20E-13	4,74E-11	9,90E-11	±5,18E-12
4	858	17,5	1,50E-08	±4,00E-12	1,45E-08	2,87E-09	±2,60E-12	9,81E-11	±2,70E-13	6,40E-11	8,78E-11	±3,58E-12
5	894	9,5	8,32E-09	±4,60E-12	8,00E-09	1,56E-09	±1,70E-12	5,42E-11	±1,90E-13	3,56E-11	5,80E-11	±3,90E-12
6	951	4,5	4,18E-09	±8,30E-13	3,41E-09	7,30E-10	±7,10E-13	2,60E-11	±2,60E-13	1,70E-11	3,62E-11	±5,48E-12
7	1024	5,8	5,28E-09	±6,10E-13	4,96E-09	9,44E-10	±8,50E-13	3,19E-11	±1,50E-13	2,06E-11	3,36E-10	±3,77E-12
8	1077	7,4	6,76E-09	±5,60E-13	6,17E-09	1,22E-09	±1,10E-12	4,25E-11	±2,20E-13	2,79E-11	2,94E-10	±4,74E-12
9	1140	12,5	1,08E-08	±7,50E-13	1,03E-08	2,04E-09	±1,80E-12	6,95E-11	±2,60E-13	4,51E-11	1,51E-10	±3,88E-12
10	1185	8,8	7,89E-09	±8,20E-13	7,36E-09	1,44E-09	±1,30E-12	4,92E-11	±2,00E-13	3,20E-11	2,84E-10	±3,38E-12
11	1260	5,9	5,55E-09	±5,10E-13	5,04E-09	9,58E-10	±8,80E-13	3,52E-11	±2,50E-13	2,40E-11	2,33E-09	±7,65E-12
Step	**Temp. (°C)**	**^{39}Ar %**	**^{40}Ar total (ml)**	**1σ (abs.) (ml)**	**^{40}Ar* (ml)**	**^{39}Ar (ml)**	**1σ (abs.) (ml)**	**^{38}Ar (ml)**	**1σ (abs.) (ml)**	**^{38}Ar Cl (ml)**	**^{37}Ar (ml)**	**1σ (abs.) (ml)**
Sample AD20 (*grain size: 300 μm*): Orthogneissic rock – biotite (J = 0.00414, mass = 10 mg)												
1	440	1,6	5,60E-09	±4,00E-13	7,30E-10	3,29E-10	±3,50E-13	9,51E-12	±1,80E-13	2,56E-12	3,27E-11	±3,95E-12
2	493	2,8	3,95E-09	±9,40E-13	1,33E-09	5,70E-10	±5,30E-13	1,44E-11	±1,80E-13	6,01E-12	4,66E-11	±3,42E-12
3	543	6,1	5,13E-09	±4,30E-13	2,86E-09	1,23E-09	±1,10E-12	2,29E-11	±1,80E-13	7,04E-12	1,43E-11	±2,46E-12
4	573	7,4	5,44E-09	±2,00E-16	3,30E-09	1,49E-09	±1,30E-12	3,10E-11	±5,70E-14	1,22E-11	2,18E-11	±3,94E-12
5	594	4,5	2,94E-09	±2,10E-11	1,77E-09	9,11E-10	±6,40E-12	1,32E-11	±6,10E-13	1,83E-12	2,13E-10	±5,46E-12
6	646	10,1	6,51E-09	±6,80E-13	4,70E-09	2,03E-09	±1,80E-12	4,72E-11	±1,80E-13	2,22E-11	2,92E-11	±3,95E-12
7	699	6,8	4,90E-09	±6,70E-13	3,31E-09	1,37E-09	±1,20E-12	2,67E-11	±1,80E-13	9,54E-12	3,68E-11	±3,15E-12
8	750	3,9	3,62E-09	±7,00E-13	1,21E-09	7,88E-10	±7,30E-13	1,70E-11	±1,80E-13	6,18E-12	7,38E-11	±3,78E-12
9	828	5,6	4,21E-09	±2,70E-13	2,27E-09	1,13E-09	±10,00E-13	2,05E-11	±1,60E-13	5,93E-12	5,46E-11	±2,21E-12
10	896	10,2	6,70E-09	±5,30E-13	4,24E-09	2,04E-09	±1,80E-12	3,52E-11	±2,00E-13	9,63E-12	1,79E-10	±3,77E-12
11	960	17,1	1,01E-08	±1,40E-12	7,76E-09	3,44E-09	±3,00E-12	5,88E-11	±2,40E-13	1,69E-11	1,02E-10	±3,44E-12
12	1018	13,3	8,14E-09	±6,10E-13	6,34E-09	2,67E-09	±2,40E-12	4,38E-11	±10,00E-14	1,12E-11	1,07E-10	±3,74E-12
13	1067	7,9	5,40E-09	±3,00E-13	3,57E-09	1,59E-09	±1,40E-12	2,79E-11	±2,10E-13	8,04E-12	2,06E-10	±1,99E-12
14	1150	1,9	2,27E-09	±2,70E-13	7,517E-10	3,83E-10	±3,60E-13	8,090E-12	±1,50E-13	2,656E-12	2,77E-10	±3,83E-12
15	1382	0,6	1,67E-09	±9,50E-13	1,06E-10	1,30E-10	±2,00E-13	4,31E-12	±2,80E-13	1,81E-12	1,72E-10	±5,98E-12
Step	**Temp. (°C)**	**^{39}Ar %**	**^{40}Ar total (ml)**	**1σ (abs.) (ml)**	**^{40}Ar* (ml)**	**^{39}Ar (ml)**	**1σ (abs.) (ml)**	**^{38}Ar (ml)**	**1σ (abs.) (ml)**	**^{38}Ar Cl (ml)**	**^{37}Ar (ml)**	**1σ (abs.) (ml)**
Sample ACIIh (*grain size: 30 μm*): Mylonitic rock – biotite (J = 0.00657, mass = 10.46 mg)												
1	444	3,1	6,59E-09	±1,90E-13	1,40E-09	9,18E-10	±8,40E-13	3,43E-11	±2,50E-13	2,02E-11	2,44E-11	±1,79E-12
2	497	2,5	2,85E-09	±2,40E-13	1,30E-09	7,67E-10	±7,40E-13	2,19E-11	±2,00E-13	1,19E-11	9,98E-12	±2,34E-12
3	545	7,2	6,05E-09	±2,80E-13	3,68E-09	2,16E-09	±1,90E-12	5,57E-11	±2,50E-13	2,88E-11	2,06E-11	±2,59E-12
4	575	8,6	6,30E-09	±10,00E-13	4,70E-09	2,59E-09	±2,30E-12	6,68E-11	±2,30E-13	3,53E-11	2,28E-11	±3,11E-12
5	606	7,8	5,95E-09	±3,00E-12	4,37E-09	2,35E-09	±2,20E-12	6,27E-11	±1,80E-13	3,41E-11	2,04E-11	±3,64E-12
6	666	13,3	8,35E-09	±7,20E-13	7,16E-09	4,02E-09	±3,60E-12	1,05E-10	±3,10E-13	5,67E-11	3,01E-11	±3,81E-12
7	718	8,9	5,98E-09	±7,00E-13	4,70E-09	2,67E-09	±2,40E-12	6,51E-11	±3,70E-13	3,28E-11	4,62E-11	±4,81E-12
8	288	2,0	3,68E-09	±2,70E-13	1,06E-09	5,93E-10	±5,60E-13	1,66E-11	±2,90E-13	8,00E-12	2,31E-11	±3,56E-12
9	765	3,3	2,51E-09	±2,50E-13	1,54E-09	9,88E-10	±9,10E-13	2,22E-11	±2,10E-13	1,00E-11	2,11E-11	±3,61E-12
10	838	8,0	5,60E-09	±1,60E-12	3,87E-09	2,39E-09	±2,10E-12	5,27E-11	±1,70E-13	2,34E-11	1,41E-10	±3,23E-12
11	910	11,8	9,14E-09	±1,50E-12	6,21E-09	3,55E-09	±3,30E-12	8,74E-11	±2,30E-13	4,38E-11	1,24E-10	±9,93E-13
12	972	15,8	1,21E-08	±8,70E-13	8,43E-09	4,77E-09	±4,20E-12	1,24E-10	±2,90E-13	6,51E-11	8,36E-11	±3,58E-12
13	1088	7,5	6,24E-09	±4,30E-13	4,45E-09	2,25E-09	±2,00E-12	5,89E-11	±2,40E-13	3,13E-11	1,32E-10	±2,70E-12
14	1170	0,3	9,18E-10	±1,50E-13	–9,446E-11	8,66E-11	±2,20E-13	3,314E-12	±2,40E-13	1,667E-12	8,29E-11	±3,68E-12
Step	**Temp. (°C)**	**^{39}Ar %**	**^{40}Ar total (ml)**	**1σ (abs.) (ml)**	**^{40}Ar* (ml)**	**^{39}Ar (ml)**	**1σ (abs.) (ml)**	**^{38}Ar (ml)**	**1σ (abs.) (ml)**	**^{38}Ar Cl (ml)**	**^{37}Ar (ml)**	**1σ (abs.) (ml)**
Sample ACIIh (*grain size: 30 μm*): Mylonitic rock – phengite (J = 0.00657, mass = 11.18 mg)												
1	440	3,3	1,01E-08	±1,80E-13	1,27E-09	1,05E-09	±9,50E-13	4,44E-11	±2,50E-13	2,65E-11	3,20E-11	±1,10E-12
2	493	2,0	2,89E-09	±1,70E-13	8,74E-10	6,51E-10	±6,30E-13	1,97E-11	±2,80E-13	1,08E-11	9,50E-12	±8,14E-13
3	542	4,7	4,98E-09	±9,50E-13	2,35E-09	1,53E-09	±1,60E-12	3,97E-11	±2,60E-13	2,00E-11	1,79E-11	±5,37E-13
4	600	9,2	7,90E-09	±7,60E-13	4,99E-09	2,98E-09	±2,60E-12	8,02E-11	±2,50E-13	4,33E-11	3,97E-11	±6,27E-13
5	656	14,8	1,01E-08	±2,50E-13	7,82E-09	4,77E-09	±4,50E-12	1,09E-10	±2,90E-13	5,13E-11	5,35E-11	±1,19E-12
6	708	7,8	5,49E-09	±2,60E-13	4,16E-09	2,52E-09	±2,20E-12	5,12E-11	±1,80E-13	2,07E-11	2,65E-11	±9,71E-13
7	756	9,3	6,00E-09	±5,10E-13	3,96E-09	3,02E-09	±2,60E-12	5,28E-11	±2,30E-13	1,60E-11	6,86E-11	±9,96E-13
8	781	9,8	5,49E-09	±2,30E-13	4,31E-09	3,17E-09	±2,80E-12	4,92E-11	±2,30E-13	1,12E-11	7,98E-11	±8,89E-13
9	796	21,7	1,25E-08	±1,70E-13	9,45E-09	7,00E-09	±6,20E-12	1,08E-10	±2,60E-13	2,32E-11	1,49E-10	±1,19E-12
10	900	7,6	6,18E-09	±2,90E-13	3,48E-09	2,47E-09	±2,20E-12	4,94E-11	±2,20E-13	1,87E-11	1,34E-10	±9,25E-13
11	981	5,1	5,20E-09	±3,10E-13	3,16E-09	1,66E-09	±1,50E-12	4,20E-11	±1,60E-13	2,12E-11	1,00E-10	±1,49E-12
12	1072	4,3	4,21E-09	±9,10E-13	2,54E-09	1,37E-09	±1,20E-12	3,43E-11	±2,00E-13	1,71E-11	2,93E-10	±1,17E-12
13	1152	0,2	6,50E-10	±2,90E-13	1,16E-10	6,20E-11	±1,50E-13	2,86E-12	±2,60E-13	1,82E-12	1,49E-10	±8,67E-13

^{36}Ar (ml)	1σ (abs.) (ml)	Cl/K	1σ (abs.)	Ca/K	1σ (abs.)	Age (Ma)	1σ (abs.) (Ma)	^{39}Ar/^{40}Ar	1σ (abs.)	^{36}Ar/^{40}Ar	1σ (abs.)
9,07E-12	±2,40E-13	5,00E-03	±2,96E-05	1,30E-01	±5,20E-03	38,0	±0,4	1,45E-01	±1,50E-04	8,62E-04	±2,30E-05
9,11E-13	±2,40E-13	5,13E-03	±5,05E-05	6,44E-02	±1,20E-02	36,9	±0,5	1,90E-01	±1,90E-04	1,75E-04	±4,50E-05
3,44E-12	±2,20E-13	5,16E-03	±2,46E-05	9,37E-02	±4,90E-03	35,7	±0,2	1,88E-01	±3,10E-04	3,05E-04	±2,00E-05
1,71E-12	±2,00E-13	5,13E-03	±2,20E-05	6,12E-02	±2,50E-03	37,2	±0,2	1,92E-01	±1,80E-04	1,13E-04	±1,30E-05
1,01E-12	±2,10E-13	5,25E-03	±2,88E-05	7,43E-02	±5,00E-03	37,9	±0,3	1,87E-01	±2,20E-04	1,30E-04	±2,50E-05
2,63E-12	±2,00E-13	5,34E-03	±8,28E-05	9,92E-02	±1,50E-02	34,5	±0,6	1,75E-01	±1,70E-04	6,26E-04	±4,80E-05
1,17E-12	±2,20E-13	5,03E-03	±3,80E-05	7,13E-01	±8,00E-03	38,8	±0,5	1,79E-01	±1,60E-04	2,05E-04	±3,90E-05
2,06E-12	±2,10E-13	5,28E-03	±4,24E-05	4,83E-01	±7,80E-03	37,5	±0,4	1,80E-01	±1,70E-04	2,94E-04	±3,00E-05
1,82E-12	±2,00E-13	5,09E-03	±2,97E-05	1,48E-01	±3,80E-03	37,3	±0,2	1,89E-01	±1,70E-04	1,65E-04	±1,80E-05
1,86E-12	±2,30E-13	5,11E-03	±3,28E-05	3,95E-01	±4,70E-03	37,8	±0,3	1,82E-01	±1,70E-04	2,27E-04	±2,80E-05
2,32E-12	±2,20E-13	5,75E-03	±6,09E-05	4,88E+00	±1,60E-02	38,9	±0,4	1,72E-01	±1,60E-04	3,11E-04	±3,00E-05
^{36}Ar (ml)	1σ (abs.) (ml)	Cl/K	1σ (abs.)	Ca/K	1σ (abs.)	Age (Ma)	1σ (abs.) (Ma)	^{39}Ar/^{40}Ar	1σ (abs.)	^{36}Ar/^{40}Ar	1σ (abs.)
1,65E-11	±2,30E-13	1,79E-03	±1,29E-04	1,98E-01	±2,40E-02	16,5	±1,5	5,88E-02	±6,20E-05	2,94E-03	±4,20E-05
8,88E-12	±8,30E-14	2,42E-03	±7,29E-05	1,63E-01	±1,20E-02	17,3	±0,3	1,45E-01	±1,40E-04	2,25E-03	±2,10E-05
7,70E-12	±1,40E-13	1,32E-03	±3,41E-05	2,33E-02	±4,00E-03	17,3	±0,3	2,39E-01	±2,20E-04	1,50E-03	±2,70E-05
7,27E-12	±3,20E-13	1,89E-03	±1,30E-05	2,94E-02	±5,30E-03	16,5	±0,5	2,73E-01	±2,40E-04	1,33E-03	±5,90E-05
3,99E-12	±1,30E-13	4,62E-04	±1,55E-04	4,68E-01	±1,20E-02	14,5	±0,3	3,10E-01	±3,10E-03	1,34E-03	±4,30E-05
6,11E-12	±1,30E-13	2,52E-03	±2,07E-05	2,88E-02	±3,90E-03	17,2	±0,2	3,12E-01	±2,90E-04	9,37E-04	±2,10E-05
5,39E-12	±1,60E-13	1,60E-03	±3,07E-05	5,37E-02	±4,60E-03	17,9	±0,3	2,80E-01	±2,60E-04	1,01E-03	±3,20E-05
8,17E-12	±1,60E-13	1,81E-03	±5,33E-05	1,87E-01	±9,60E-03	11,4	±0,5	2,18E-01	±2,10E-04	2,26E-03	±4,50E-05
6,57E-12	±1,60E-13	1,20E-03	±3,31E-05	9,64E-02	±3,90E-03	14,9	±0,3	2,70E-01	±2,40E-04	1,56E-03	±3,70E-05
8,37E-12	±2,20E-13	1,09E-03	±2,31E-05	1,75E-01	±3,70E-03	15,5	±0,2	3,04E-01	±2,70E-04	1,24E-03	±3,30E-05
7,88E-12	±2,10E-13	1,13E-03	±1,64E-05	5,96E-02	±2,00E-03	16,8	±0,1	3,41E-01	±3,10E-04	7,79E-04	±2,10E-05
6,09E-12	±1,90E-13	9,69E-04	±9,46E-06	8,04E-02	±2,80E-03	17,7	±0,2	3,28E-01	±3,00E-04	7,45E-04	±2,30E-05
6,27E-12	±1,30E-13	1,16E-03	±3,07E-05	2,59E-01	±2,50E-03	16,7	±0,2	2,94E-01	±2,60E-04	1,15E-03	±2,40E-05
5,214E-12	±1,80E-13	1,59E-03	±9,22E-05	1,44E+00	±2,00E-02	14,6	±1,0	1,69E-01	±1,60E-04	2,26E-03	±7,90E-05
5,34E-12	±2,60E-13	3,21E-03	±5,02E-04	2,64E+00	±9,20E-02	6,1	±4,3	7,78E-02	±1,30E-04	3,17E-03	±1,50E-04
^{36}Ar (ml)	1σ (abs.) (ml)	Cl/K	1σ (abs.)	Ca/K	1σ (abs.)	Age (Ma)	1σ (abs.) (Ma)	^{39}Ar/^{40}Ar	1σ (abs.)	^{36}Ar/^{40}Ar	1σ (abs.)
1,76E-11	±1,70E-13	5,06E-03	±6,32E-05	5,31E-02	±3,90E-03	18,0	±0,6	1,39E-01	±1,30E-04	2,67E-03	±2,50E-05
5,24E-12	±1,20E-13	3,56E-03	±6,04E-05	2,60E-02	±6,10E-03	20,0	±0,6	2,69E-01	±2,60E-04	1,84E-03	±4,30E-05
8,03E-12	±2,40E-13	3,07E-03	±2,71E-05	1,90E-02	±2,40E-03	20,1	±0,4	3,57E-01	±3,20E-04	1,33E-03	±4,00E-05
5,40E-12	±1,50E-13	3,13E-03	±2,07E-05	1,76E-02	±2,40E-03	21,4	±0,2	4,12E-01	±3,70E-04	8,57E-04	±2,40E-05
5,36E-12	±1,40E-13	3,35E-03	±1,80E-05	1,74E-02	±3,10E-03	21,9	±0,2	3,94E-01	±4,30E-04	9,00E-04	±2,40E-05
4,02E-12	±1,40E-13	3,25E-03	±1,80E-05	1,50E-02	±1,90E-03	21,0	±0,1	4,81E-01	±4,30E-04	4,81E-04	±1,70E-05
4,32E-12	±2,00E-13	2,83E-03	±3,21E-05	3,46E-02	±3,60E-03	20,7	±0,3	4,47E-01	±4,00E-04	7,22E-04	±3,30E-05
8,86E-12	±1,70E-13	3,10E-03	±1,13E-04	7,79E-02	±1,20E-02	21,0	±1,0	1,61E-01	±1,50E-04	2,41E-03	±4,70E-05
3,30E-12	±1,70E-13	2,33E-03	±4,95E-05	4,26E-02	±7,30E-03	18,3	±0,6	3,94E-01	±3,60E-04	1,31E-03	±6,60E-05
5,92E-12	±1,30E-13	2,25E-03	±1,67E-05	1,18E-01	±2,70E-03	19,0	±0,2	4,27E-01	±4,00E-04	1,05E-03	±2,40E-05
9,95E-12	±2,00E-13	2,84E-03	±1,53E-05	6,99E-02	±5,60E-04	20,6	±0,2	3,88E-01	±3,70E-04	1,08E-03	±2,20E-05
1,24E-11	±1,30E-13	3,14E-03	±1,42E-05	3,50E-02	±1,50E-03	20,8	±0,1	3,95E-01	±3,50E-04	1,02E-03	±1,10E-05
6,10E-12	±2,10E-13	3,20E-03	±2,50E-05	1,18E-01	±2,40E-03	23,3	±0,3	3,61E-01	±3,20E-04	9,73E-04	±3,40E-05
3,446E-12	±2,10E-13	4,43E-03	±6,46E-04	1,92E+00	±8,50E-02	–13,0	±–8,5	9,43E-02	±2,40E-04	3,73E-03	±2,30E-04
^{36}Ar (ml)	1σ (abs.) (ml)	Cl/K	1σ (abs.)	Ca/K	1σ (abs.)	Age (Ma)	1σ (abs.) (Ma)	^{39}Ar/^{40}Ar	1σ (abs.)	^{36}Ar/^{40}Ar	1σ (abs.)
2,97E-11	±1,80E-13	5,79E-03	±5,53E-05	6,09E-02	±2,10E-03	14,3	±0,6	1,05E-01	±9,40E-05	2,95E-03	±1,80E-05
6,81E-12	±2,10E-13	3,82E-03	±9,99E-05	2,92E-02	±2,50E-03	15,8	±1,1	2,26E-01	±2,20E-04	2,36E-03	±7,20E-05
8,92E-12	±3,00E-13	3,00E-03	±4,00E-05	2,34E-02	±7,00E-04	18,1	±0,7	3,08E-01	±3,30E-04	1,79E-03	±6,10E-05
9,86E-12	±1,50E-13	3,34E-03	±1,95E-05	2,66E-02	±4,20E-04	19,7	±0,2	3,78E-01	±3,30E-04	1,25E-03	±1,90E-05
7,63E-12	±2,00E-13	2,48E-03	±1,43E-05	2,24E-02	±5,00E-04	19,3	±0,1	4,74E-01	±4,40E-04	7,56E-04	±1,90E-05
4,51E-12	±2,40E-13	1,88E-03	±1,71E-05	2,10E-02	±7,70E-04	19,4	±0,3	4,59E-01	±4,10E-04	8,20E-04	±4,30E-05
6,93E-12	±1,90E-13	1,22E-03	±1,79E-05	4,55E-02	±6,60E-04	15,5	±0,2	5,03E-01	±4,40E-04	1,15E-03	±3,20E-05
4,01E-12	±2,00E-13	8,08E-04	±1,71E-05	5,03E-02	±5,60E-04	16,0	±0,2	5,78E-01	±5,10E-04	7,26E-04	±3,70E-05
1,04E-11	±2,20E-13	7,64E-04	±8,98E-06	4,26E-02	±3,40E-04	15,9	±0,1	5,59E-01	±4,90E-04	8,29E-04	±1,70E-05
9,16E-12	±1,80E-13	1,75E-03	±2,09E-05	1,08E-01	±7,50E-04	16,7	±0,3	3,99E-01	±3,50E-04	1,48E-03	±2,90E-05
6,93E-12	±1,40E-13	2,94E-03	±2,26E-05	1,22E-01	±1,80E-03	22,4	±0,3	3,19E-01	±2,80E-04	1,33E-03	±2,60E-05
5,74E-12	±1,80E-13	2,87E-03	±3,40E-05	4,26E-01	±1,70E-03	21,8	±0,4	3,26E-01	±3,00E-04	1,35E-03	±4,10E-05
1,85E-12	±2,10E-13	6,74E-03	±9,75E-04	4,81E+00	±2,80E-02	22,0	±11,0	9,53E-02	±2,30E-04	2,78E-03	±3,10E-04

size: 18 Ma for the weakly deformed rock and orthogneiss, and 16 Ma (model 1) or 11 Ma (model 2) for the mylonitic rock (triangles, Fig. 7). A similar trend would be expected for phengites (circles, Fig. 7) using the diffusion coefficient and activation energy of 0.11 cm^2/s and 250 kJ/mol, respectively (Hames and Cheney 1997). Thus, significantly younger ages would be expected for smaller grains.

In both sampling profiles, no correlation between ^{39}Ar-^{40}Ar biotite ages and strain intensity or grain size is observed. Except for the Aar 31 biotite, all isochemical mica ages in orthogneisses and mylonites are bracketed between 21 and 17 Ma (Fig. 6). These results are younger than the maximum permissible stratigraphic age of 34 Ma and concordant with the modelled metamorphic age of the ECM (23–18 Ma, Figs. 4c, and f). This argues against significant excess Ar. Furthermore, the comparatively tight age distribution of the six inheritance-free micas also argues against a large influence of excess Ar (e.g. see Brewer 1969).

Rb-Sr data

In the Grimsel granodiorite profile, the undeformed rock (Aar 31 = AD 13) was analyzed by Marquer and Peucat (1994) and is shown here for completeness. Inter-mineral isotopic disequilibrium can be seen in the weakly deformed rock and the orthogneissic rock in the shear zone profile of the Grimsel granodiorite (Fig. 8). In the Rb-Sr isochron plot, only the Grimsel granodiorite mylonitic rock exhibits a statistically "acceptable" alignment of the data points (AC II h:WR, phengite and biotite). Apparent Rb/Sr whole rock-biotite ages are 15.9 ± 0.4, 22.4 ± 2.5 and 12.2 ± 1.3 Ma for the three rock types in the Grimsel granodiorite shear zone profile (Fig. 8 and Table 4). The last, more highly strained sample gives a whole rock-phengite age of 12.6 ± 0.3 Ma (Fig. 8 and Table 4). Thus, these two whole rock-mica ages give concordant results around 12.5 Ma.

For the mylonitic rock in the Aar granite, the whole rock-biotite age is 10.1 ± 0.3 Ma whereas the whole rock-phengite age is negative, which is proof of initial isotopic disequilibrium (Table 4 and Fig. 8). As deformation progresses, the whole-rock point becomes more enriched in Rb and in ^{87}Sr (compare Aar10 and Aar 17, Fig. 8). This requires an open system with chemical mass-transfer and large fluid circulations (Marquer and Peucat 1994).

Rb-Sr interpretation

Rb-Sr ages were determined for two reasons: i) to compare with the often-quoted data presented by Jaeger and co-workers and reviewed by Hunziker et al. (1992) and ii) to assess whether such samples fully satisfy the prerequisite of Rb-Sr dating, i.e. internal isotopic equilibrium.

The whole rock Rb-Sr isotopic dating method, applied to greenschist-facies shear zones in the ECM, was previously investigated by Marquer and Peucat (1994). These authors analysed weakly deformed rocks of the Aar granite and the Grimsel granodiorite with the aim of determining their magmatic age. Their Rb-Sr isochron age was concordant with Upper Carboniferous zircon U-Pb ages (Schaltegger 1994). However, orthogneissic and mylonitic rocks yielded a large scatter of Rb-Sr ages and were aligned, from weakly deformed to orthogneissic and mylonitic rocks, along a geologically meaningless „errorchron", giving fictitious Early Cretaceous ages. This suggested that isotopic homogenisation was not reached in these shear zones and hence that the whole rock Rb-Sr isotopic dating method is not appropriated for determining geologically meaningful ages in granitic rocks that experience greenschist-facies deformation, because of the mass transfer that occurs in a chemically open system. We have attempted to understand which component of the whole-rock system is responsible for this. Furthermore, the whole-rock perturbations certainly also affect whole rock-mineral ages, and the significance of apparent ages is not obvious. Indeed, an inconsistent pattern is revealed by the whole rock-biotite data: the weakly deformed sample (25.1 ± 0.7 Ma) and the mylonitic rock (10.1 ± 0.3 Ma) give two different "ages" for the same 450 °C deformation event. Furthermore, the three whole rock-biotite ages do not show systematically decreasing values with decreasing grain size in the Grimsel granodiorite samples. Moreover, considering the mylonites in the Grimsel granodiorite, the whole rock-biotite age (12.2 ± 1.3 Ma) is close to the whole rock-phengite age (12.6 ± 0.3 Ma) while "thermochronology" requires drastically different "closure temperatures" values for these two minerals, namely 300 ± 50 °C and 500 ± 50 °C, respectively (Hunziker et al. 1992). If these ages were interpreted using the conventional "closure temperature" hypothesis, this result would imply an unrealistic, ultra-fast temperature drop of 200 °C between 12.6 and 12.2 Ma. To escape that paradox, in principle one could extend the conventional approach and interpret the mylonite ages as formation ages, implying that

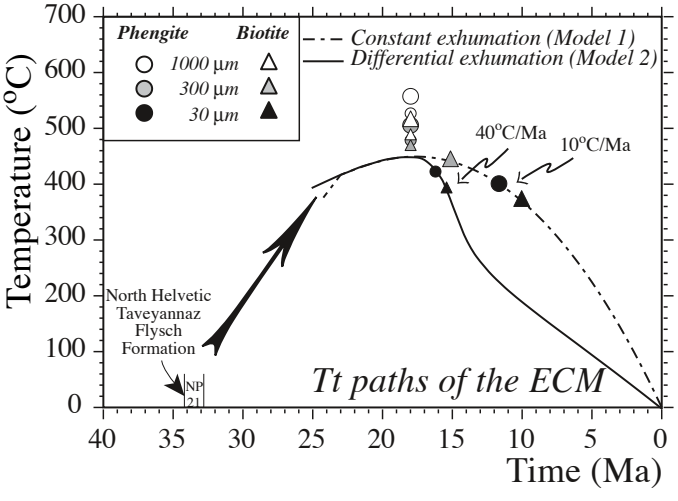

Fig. 7. Calculated "closure temperatures" for K-Ar in micas versus grain size, projected onto the modelled T-t paths for the ECM. Retrograde paths: dashed line: model 1 (Fig. 4c); solid line: model 2 (Fig. 4f).

Tab. 4. Rb-Sr results from the External Crystalline Massifs.

Sample		Rb [ppm]	Sr [ppm]	$^{87}Rb/^{86}Sr$	2σ (abs)	$^{87}Sr/^{86}Sr$	2σ (abs)		Age [Ma]	2σ (abs)	Intercept	2σ (abs)	M.S.W.D.
Aar granite													
Weakly deformed rock (grain size: 1000 μm)													
Aar10	WR	214	79	7,806979	±0,010825	0,731928	±0,000028						
	Bt	1166	100	33,915499	±0,605921	0,741252	±0,000167	WR-Bt	25,1	±0,7	0,7291	±0,0001	2 pt
Mylonitic rock (grain size: 30 μm)													
Aar17	WR	396	71	16,152830	±0,010657	0,744057	±0,000056						
	Bt	210	13	47,504246	±0,022223	0,748567	±0,000098	WR-Bt	10,1	±0,3	0,7417	±0,0001	2 pt
	Phe	172	6	81,136672	±0,213129	0,732672	±0,000244						
	Phe"	63	4	44,647915	±0,033370	0,735040	±0,000039	WR-Phe	negative				2 pt
Grimsel granodiorite													
Weakly deformed rock (grain size: 1000 μm)													
AD13	WR*	115	399	0,840000	±0,004200	0,708950	±0,000079						
	Bt*	552	55	29,300000	±0,150000	0,715370	±0,000158	WR*-Bt*	15,9	±0,4	0,7088	±0,0001	2 pt
Orthogneissic rock (grain size: 300 μm)													
AD20	WR	149	235	1,836146	±0,001976	0,710093	±0,000029						
	Bt	566	126	13,024662	±0,024467	0,713651	±0,000394	WR-Bt	22,4	±2,5	0,7095	±0,0001	2 pt
Mylonitic rock (grain size: 30 μm)													
AD20	Bt*	608	29	60,800000	±0,304000	0,720660	±0,000360						
ACIIh	WR	218	225	2,800116	±0,005038	0,711382	±0,000053						
	Bt	551	64	25,074639	±0,041008	0,715351	±0,000074	WR-Bt-Bt*	12,2	±1,3	0,7109	±0,0003	25,2
	Phe	452	68	19,122276	±0,012198	0,714308	±0,000038	WR-Phe	12,6	±0,3	0,7109	±0,0001	2 pt

*Rennes University analyses, 1987.

biotites and phengites both grew at ca. 12.5 Ma below 300 °C, ca. 5–8 Ma later than the micas in weakly deformed rocks of the same shear zone. However, the microstructural observations and the petrological constraints (such as the Si content of white mica) rule out such a diachronous growth, and indeed the K-Ar system does not record it either.

The Grimsel granodiorite and Aar granite Rb-Sr WR results demonstrate that the whole rock system is not the most retentive one, as postulated by the conventional closure temperature approach (Hunziker et al. 1992). For whole rock-biotite ages, we observe a lack of correlation between ages and strain intensity and between ages and grain size. This means that ages in deformed rocks are not simply controlled by grain size reduction. Furthermore, shear zones are interconnected pathways open to late fluid circulation and thus partial resetting of Rb-Sr systematics is expected to occur by chemical exchange, independent of temperature (see Marquer 1987; Marquer & Burkhard 1992; McCaig 1997). We propose that, in a chemically open system, it is the extent of recrystallisation which determines the resetting of isotopic systems. Thus, we do not observe Sr isotopic equilibrium because the different minerals have recrystallised to different degrees at the time of late fluid circulations.

Discussion

In the rocks sampled across progressively deformed profiles, the Rb-Sr and ^{39}Ar-^{40}Ar dates scatter within Oligo-Miocene time, but do not present a systematic correlation with either strain intensity or grain size (Fig. 9). In deformed samples, biotite and phengite yield similar ages for each isotopic method: 21–17 Ma by ^{39}Ar-^{40}Ar and 12–10 Ma by Rb-Sr. These new isotopic observations in metamorphic shear zones cannot be reconciled with the hypothesis that mineral ages are controlled by temperature. If that were true, the calculated T-t history would be mirrored by the age results in Fig. 7.

^{39}Ar-^{40}Ar biotite and white mica ages give results (21–17 Ma) in approximate agreement with the calculated timing of peak *T* conditions, regardless of their mineral grain size, while Rb-Sr whole rock-mineral ages scatter from ages corresponding to peak *T* conditions to young ages at around 10 Ma in mylonites (Fig. 9). These "young" ages cannot be reconciled with either geological age estimates or P-T modelling. In the shear zones, a strong decrease in the grain size and the degree of interconnection of small-scale shear planes enhanced syn-metamorphic fluid circulation (Marquer 1989). From major element and stable isotope mobility in the Grimsel granodiorite, theoretical calculations suggest that these metamorphic ductile shear zones were infiltrated by around 10^5 moles H_2O/cm^2, with a fluid flow in the direction of decreasing temperature (Dipple & Ferry 1992). This result is compatible with the fact that, in the major thrusts, rocks located in the overlying Helvetic cover were affected and contaminated by fluid circulations coming from the underlying basement (Marquer & Burkhard 1992). The average flow rate and in situ permeabil-

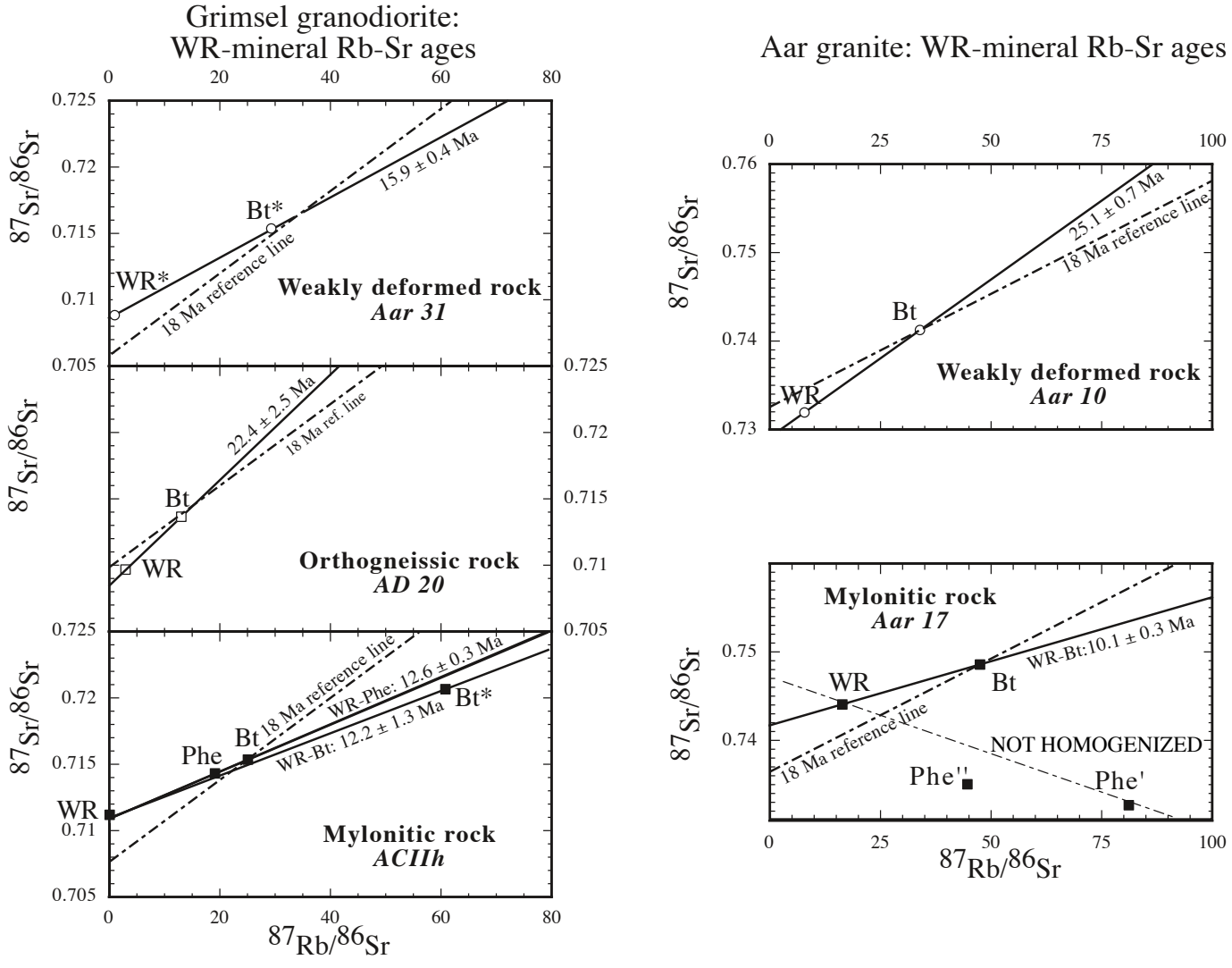

Fig. 8. Rb-Sr isochron plots for the Aar granite and Grimsel granodiorite samples. Bold dashed lines: 18 Ma reference lines corresponding to first (a) fluid inclusion generation age (recalculated after Mullis (1996); Fig. 4b and e). Bt*: analyses performed at the University of Rennes on different separates (Tab. 4).

ity were evaluated as 10^{-1}-10^{-3} m/a and 10^{-15}–10^{-17} m^2, respectively, which emphasises the fact that mylonite zones are more permeable than rocks affected by regional metamorphism (Dipple & Ferry 1992). Thus, ^{39}Ar-^{40}Ar mica ages between 21–17 Ma are interpreted as crystallisation ages, during the main shearing event and at the peak temperature, assisted by syn-metamorphic fluid circulation (Fig. 9 and 10). Neither the peak temperature around 450 °C nor the subsequent lower-temperature history had any influence on biotite and muscovite ages.

Rb-Sr mica-whole rock apparent ages in mylonitic samples cluster around 12 to 10 Ma. From the P-T-t evolution described in model 1, it follows that the occurrence of late quartz overgrowths in extensional veins (generations b and c after Mullis 1996) had to take place at a time dictated by the intersection of the isochores with the model P-T-t curve. The timing of this intersection is variably modelled as a function of boundary conditions (Fig. 4). For our set of input parameters, model age ranges for generation b are 14–9 Ma, and for generation c 13–5 Ma (Figs. 4b, e). While these young ages in mylonites are apparently coherent with K/Ar dating of clays from a fault gouge in the same area (Kralik et al. 1992: age 10–7 Ma), it is not clear to what extent these latter ages reflect fluid flow, shearing, partial inheritance, or partial alteration in a chemically open system. Rb-Sr dates, scattering from 25 to 10 Ma, are interpreted as partially reset ages, with resetting more complete in mylonites as the result of enhanced late fluid circulation (Fig. 9). The whole rock-mineral isochrons are thus controlled by the geohygrometric events, rather than by the thermal ("cooling") history.

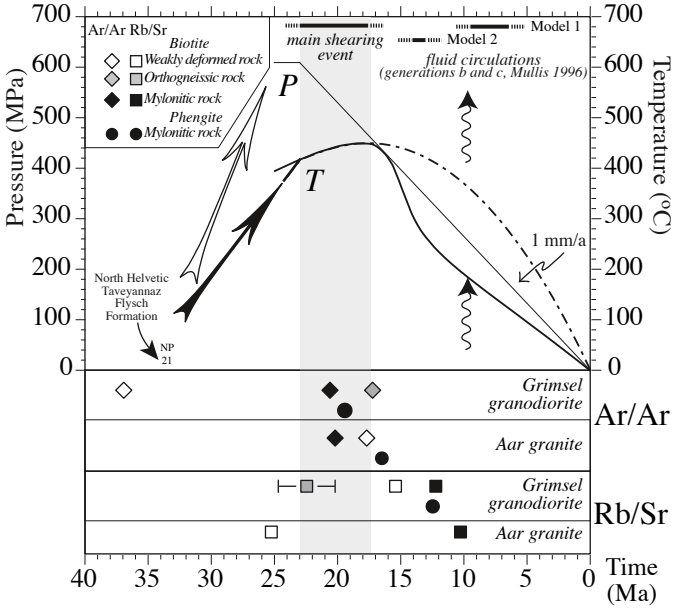

Fig. 9. ^{39}Ar-^{40}Ar isochemical age and Rb-Sr dating results correlated with the modelled Oligo-Miocene PTt path of the ECM (model 1, Fig. 4). White, grey, and black symbols correspond to weakly deformed, orthogneiss and mylonite samples, respectively.

As for the "closure temperature" hypothesis, we observe that it conflicts with the present data in two essential respects. Firstly, our geodynamic numerical model rules out an Eocene metamorphism. As pointed out by Villa (1998, his Fig. 1), decreasing the age of Central Alpine metamorphism necessarily requires that all "closure temperature" estimates must be substantially increased. In the case of the Aar massif, this increase must be at least by 150 °C to accommodate the P-T constraints. A revised set of high "closure temperatures" has the logical implication that most mineral age rejuvenations encountered in the Central Alps were not due to a sufficiently high temperature but to other processes such as recrystallisation (favoured by fluid circulation and/or deformation). Secondly, our observations of age diversity within small outcrops require that mineral ages vary independently of temperature. In summary, no Alpine mineral age can be used as a "cooling age" to constrain paleo-temperatures, "cooling histories" or exhumation rates in rocks affected by large-scale fluid circulations.

The Rb-Sr apparent ages around 12–10 Ma are unlikely to be true ages solely due to mica recrystallization, as that would imply that the whole rock remained unperturbated, and would also imply that the K-Ar system would be similarly affected. On the contrary, a significant mass transfer is certain to have affected the whole rocks (see above and Marqueur and Pencar, 1994). This event can be associated with the "b" and "c" fluid circulation events described on Fig. 4. These may be fluids that were expelled during burial of the European crust below the Aar massif, as the Jura belt began to form (Fig. 10). The P-T-t paths related to model 1 and model 2 give the youngest (9–7 Ma) and the oldest (14–13 Ma) time conditions for late fluid circulation that could have occurred in ECM (Fig. 4). The fluids expelled during progressive under-thrusting of the European crust and the time delay needed to heat up and dehydrate these buried basement rocks could explain the difference in age between the beginning of the Jura formation at around 12 Ma and the migration of metamorphic fluids through the ECM.

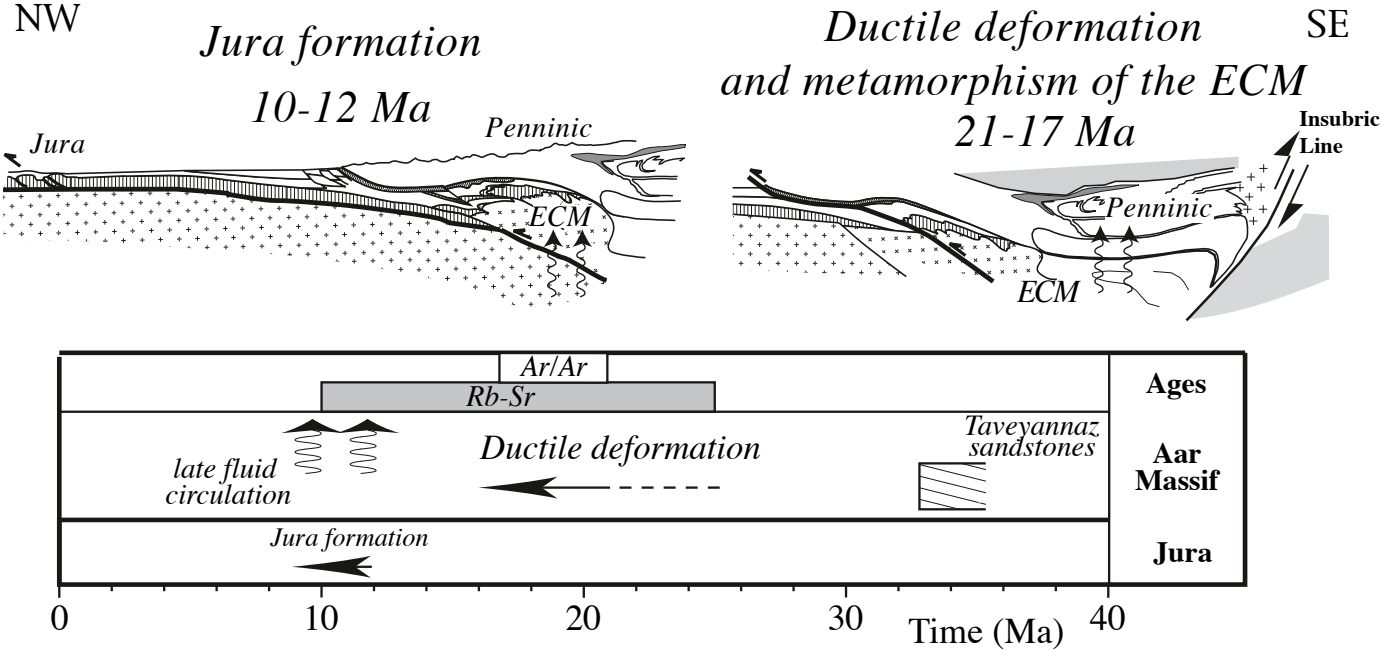

Fig. 10. Correlation between mineral ages, ductile deformation of the ECM, Jura formation and fluid circulation in the external part of the Swiss Alps.

Conclusions

Our results provide new constraints on the Oligo-Miocene tectono-metamorphic evolution of the External Crystalline Massifs. The age of the last stages of ductile deformation in the basement of the ECM can now be bracketed between 21 and 17 Ma using ^{39}Ar-^{40}Ar isochemical dates in orthogneisses and mylonites, which appear to be less sensitive to partial resetting and inheritance. These isotopic dates correspond to the calculated peak T conditions in the one-dimensional P-T-t path model constructed independently from isotopic results. These new results fit with the tectonic evolution proposed for the Helvetic system (Burkhard 1988).

The results of Rb-Sr dating in shear zones are likely to reflect late fluid circulation. Our data on the Aar massif conclusively show that temperature is not the main limiting parameter of isotopic closure for metagranites deformed during a low-grade metamorphic event and that fluid circulation plays a major role in isotopic resetting. Simple application of the "closure temperature" concept predicts different Rb-Sr ages for biotite-phengite isochrons from those observed. Furthermore, this study shows that the ^{39}Ar-^{40}Ar method can be used to constrain the timing of the ductile deformation at peak temperature to have occurred around 17–21 Ma. Disturbance of the Rb-Sr system by fluid circulation resulted in apparent whole rock-biotite Rb-Sr ages discordant with the ^{39}Ar-^{40}Ar ages. The Rb-Sr whole rock-mica ages of 10–12 Ma in the shear zones certainly do not date a pure "cooling" and instead are perturbated by the late hygrometric event documented by fluid inclusion studies. This could be linked to the expulsion of deep fluids during the under-thrusting of European continental crust below the ECM, synchronous with the formation of the Jura belt.

Acknowledgements

This paper is dedicated to the memory of Martin Burkhard for the enthusiastic and helpful discussions we had at the University of Neuchâtel. This work was part of the PhD project of N.C. (1996–2000). Isotope research in Bern was partly funded by SNF grant n° 20.47157-96. We would like to thank R. Hosein for correcting the English in this manuscript, T. Adatte for his help with time scales, N. Mancktelow for providing the modelling code, R. Brunner for mass spectrometer maintenance. The authors would finally thank R. Spikings, A. Steck, W. Müller and N. Mancktelow for their constructive remarks about the manuscript.

REFERENCES

Abrecht, J. 1994: Geologic units of the Aar Massif and their pre-Alpine rock associations: a critical review. The pre-Alpine crustal evolution of the Aar, Gotthard and Tavetsch massifs. Schweizerische Mineralogische und Petrographische Mitteilungen 74, 5–27.

Bambauer, H.U. & Bernotat, W.H. 1982: The microcline/sanidine transformation isograd in metamorphic regions: I, Composition and structural state of alkali feldspars from granitoid rocks of two N-S traverses across the Aar Massif and Gothard „Massif", Swiss Alps. Schweizerische Mineralogische und Petrographische Mitteilungen 62, 185–230.

Belluso, E., Ruffini, R., Schaller, M. & Villa, I.M. 2000: Electron-microscope and Ar isotope characterization of chemically heterogeneous amphiboles from the Palala Shear Zone, Limpopo Belt, South Africa. European Journal of Mineralogy 12, 45–62.

Berggren, W.A., Kent, D.V., Swisher, C.C., & Aubry, M.P. 1995: A revised Cenozoic geochronology and chronostratigraphy. In: Berggren, W.A., Kent, D.V., Aubry, M.P. & Hardenbol. J. (Eds.): Geochronology, time scales and global stratigraphic correlation. Special Publication – SEPM (Society for Sedimentary Geology) 54, 129–212.

Bernotat, W. & Bambauer, H.U. 1980: Die Mikroklin/Sanidin-Isograde in Aar- und Gotthardmassiv. Eclogae Geologicae Helvetiae 73, 559–561.

Bernotat, W.H. & Bambauer, H.U. 1982: The microcline/sanidine transformation isograd in metamorphic regions: II, The region of Lepontine metamorphism, Central Swiss Alps. Schweizerische Mineralogische und Petrographische Mitteilungen 62, 231–244.

Brereton, N.R. 1970: Corrections for interfering isotopes in the ^{40}Ar/^{39}Ar dating method. Earth and Planetary Science Letters 8, 427–433.

Brewer, M.S. 1969: Excess radiogenic argon in metamorphic micas from the eastern Alps, Austria. Earth and Planetary Science Letters 6, 321–331.

Brix, M.R., Stöckhert, B., Seidel, E., Theye, T., Thomson, S.N. & Kuster, M. 2002: Thermobarometric data from a fossil zircon partial annealing zone in high pressure-low temperature rocks of eastern and central Crete, Greece. Tectonophysics 349, 309–326.

Burkhard, M. 1988: L'Hélvetique de la bordure occidentale du massif de l'Aar (évolution tectonique et métamorphique) Eclogae Geologicae Helvetiae 81, 63–114.

Carpéna, J. 1992: Fission track dating of zircon; zircons from Mont Blanc Granite (French-Italian Alps). Journal of Geology 100, 411–421.

Challandes, N., Marquer, D., & Villa, I. M. 2003: Dating the evolution of C-S microstructures: a combined ^{39}Ar-^{40}Ar step-heating and UV laser-probe analysis of the Alpine Roffna shear zone. Chemical Geology 197, 3–19.

Choukroune, P. & Gapais, D. 1983: Strain pattern in the Aar Granite (Central Alps): orthogneiss developed by bulk inhomogeneous flattening. Journal of Structural Geology 5, 411–418.

Coyle, D.A. & Wagner, G.A. 1998: Positioning the titanite fission-track partial annealing zone. Chemical Geology 149, 117–125.

Crespo-Blanc, A., Masson, H., Sharp, Z., Cosca, M. & Hunziker, J. 1995: A stable and ^{40}Ar/^{39}Ar isotope study of a major thrust in the Helvetic nappes (Swiss Alps): evidence for fluid flow and constraints on nappe kinematics. Geological Society of America Bulletin 107, 1129–1144.

Davy, P. & Gillet, P. 1986: The stacking of thrust slices in collision zones and its thermal consequences. Tectonics 5, 913–929.

Dempster, T.J. 1986: Isotope systematics in minerals: biotite rejuvenation and exchange during Alpine metamorphism. Earth and Planetary Science Letters 78, 355–367.

Dipple, G.M. & Ferry, J.M. 1992: Metasomatism and fluid flow in ductile fault zones. Contributions to Mineralogy and Petrology 112, 149–164.

Di Vincenzo, G., Vitiri, C. & Rocchi, S. 2003: The effect of chlorite interlayering on ^{40}Ar-^{39}Ar dating: an ^{40}Ar-^{39}Ar laser-probe and TEM investigations of variably chloritised biotites. Contributions to Mineralogy and Petrology 145, 643–658.

Dodson, M.H. 1973: Closure Temperature in Cooling Geochronological and Petrological Systems. Contributions to Mineralogy and Petrology 40, 259–274.

Dolivo, E. 1982: Nouvelles observations structurales au SW du massif de l'Aar entre Visp et Gampel. Beiträge zur Geologischen Karte der Schweiz (NF) 157.

Escher, A., Hunziker, J., Marthaler, M., Masson H., Sartori, M. & Steck, A.1997: Geological framework and structural evolution of the western Swiss-Italian Alps. In: Pfiffner, O.A., Lehner, P., Heitzmann, P., Mueller, S. & Steck, A. (Eds.): Deep structure of the Swiss Alps: Results of NRP 20. Birkhäuser Verlag, Basel, 205–221.

England, P.C. & Richardson, S.W. 1977: The influence of erosion upon the mineral facies of rocks from different metamorphic environments. Journal of the Geological Society of London 134, Part 2, 201–213.

England, P.C. & Thompson, A.B. 1984: Pressure-temperature-time paths of regional metamorphism. I. Heat transfer during the evolution of a region of thickened continental crust. Journal of Petrology 25, 894–928.

Fischer, H., Villa, I.M., 1990: Erste K/Ar und $^{40}Ar/^{39}Ar$ -Hornblende-Mineralalter des Taveyannaz-Sandsteins. Schweizerische Mineralogische und Petrographische Mitteilungen 70, 73–75.

Fourcade, S., Marquer, D. & Javoy, M. 1989: $^{18}O/^{16}O$ variations and fluid circulation in a deep shear zone: the case of the Alpine ultramylonites from the Aar Massif (Central Alps, Switzerland). Chemical Geology 77, 119–131.

Frey, M., Bucher, K., Frank, E. & Mullis, J. 1980: Alpine metamorphism along the Geotraverse Basel-Chiasso: a review. Eclogae Geologicae Helvetiae 73, 527–546.

Frey, M., Hunziker, J.C., Frank, W., Bocquet, J., Dal Piaz, G.V., Jaeger, E. & Niggli, E. 1974: Alpine metamorphism of the Alps: a review. Schweizerische Mineralogische und Petrographische Mitteilungen 54, 247–290.

Frey, M. & Ferreiro Mählmann, R. 1999: Alpine metamorphism of the Central Alps. Schweizerische Mineralogische und Petrographische Mitteilungen 79, 135–154.

Gapais, D., Bale, P., Choukroune, P., Cobbold, P.R., Mahjoub, Y. & Marquer, D. 1987: Bulk kinematics from shear zone patterns: some field examples. Journal of Structural Geology 9, 635–646.

Gerya, T.V., Stöckhert, B. & Perchuk, A.L., 2002: Exhumation of high pressure metamorphic rocks in a subduction channel: a numerical simulation. Tectonics 26, 6, 1–15.

Grasemann, B. & Mancktelow, N.S. 1993: Two-dimensional thermal modelling of normal faulting: the Simplon fault zone, Central Alps, Switzerland. Tectonophysics 225, 155–165.

Hames, W.E. & Cheney, J.T. 1997: On the loss of $^{40}Ar^*$ from muscovite during polymetamorphism. Geochimica et Cosmochimica Acta 61, 3868–3872.

Hetherington, C.J. & Villa, I.M. 2007: Barium silicates of the Berisal Complex, Switzerland: a study in geochronology and rare-gas release systematics. Geochimica et Cosmochimica Acta 71, 3336–3347.

Hofmann, B.A., Helfer, M., Diamond, L.W., Villa, I., Frei, R. & Eikenberg, J. 2004: Topography-driven hydrothermal breccia mineralization of Pliocene age at Grimsel Pass, Aar Massif, Central Swiss Alps. Schweizerische Mineralogische und Petrographische Mitteilungen 84, 271–302.

Hunziker, J.C., Desmons, J. & Martinotti, G. 1992: Thirty-two years of geochronological work in the Central and Western Alps: a review on seven maps. Mémoires de Géologie, Lausanne 13, 59 pp.

Hunziker, J.C., Frey, M., Clauer, N., Dallmeyer, R.D., Friedrichsen, H., Flehmig, W., Hochstrasser, K., Roggwiler, P. & Schwander, H. 1986: The evolution of illite to muscovite: mineralogical and isotopic data from the Glarus Alps, Switzerland. Contributions to Mineralogy and Petrology 92, 157–180.

Jaeger, E., Niggli, E. & Wenk, E. 1967: Altersbestimmungen an Glimmern der Zentralalpen. Beiträge zur die Geologischen Karte der Schweiz., N.F. 134, 1–67.

Jamieson, R.A., Beaumont, C., Fullsack, P. & Lee, B. 1998: Barrovian regional metamorphism: Where's the heat? In: Treolar, P. & O'Brien, P. (Eds.): What Drives Metamorphism and Metamorphic Reactions? Geological Society of London Special Publication 138, 23–51.

Karabinos, P. & Ketcham, R. 1988: Thermal structure of active thrust belts. Journal of Metamorphic Geology 6, 559–570.

Kirschner, D.L., Sharp, Z.D. & Masson, H. 1995: Oxygen isotope thermometry of quartz-calcite veins: unraveling the thermal-tectonic history of the subgreenschist facies Morcles Nappe (Swiss Alps). Geological Society of America Bulletin 107, 1145–1156.

Kirschner, D.L., Cosca, M.A., Masson, H. & Hunziker, J.C. 1996: Staircase $^{40}Ar/^{39}Ar$ spectra of fine-grained white mica: timing and duration of deformation and empirical constraints on argon diffusion. Geology 24, 747–750.

Kralik, M., Clauer, N., Holnsteiner, R., Huemer, H. & Kappel, F. 1992: Recurrent fault activity in the Grimsel Test Site (GTS, Switzerland) revealed by Rb-Sr, K-Ar and tritium isotope techniques. Journal of the Geological Society of London 149, 293–301.

Labhart, T.P. 1977: Aarmassiv und Gotthardmassiv. Sammlung geologischer Fuehrer. Gebrüder Borntraeger, Berlin, Stuttgart, 173 pp.

Lateltin, O. & Muller, D. 1987: Evolution paléogéographique du bassin des grès de Taveyannaz dans les Aravis (Haute-Savoie) à la fin du Paléogène. Eclogae Geologicae Helveticae 80, 127–140.

Ludwig, K.R. 2000: Isoplot/Ex. Berkeley Geochronology Center, Special Publication No.1a.

Mancktelow, N.S. 1998: A stepwise discrete Fourier transform approach to 1D thermal modelling of exhumation by erosion and stretching. Computers & Geosciences 24, 829–837.

Marquer, D. 1987: Transfert de matière et déformation progressive des granitoïdes. Exemple des massifs de l'Aar et du Gothard (Alpes centrales suisses). PhD Thesis, Mémoires et Documents du Centre Armoricain d'Etudes Structurales des Socles, Université de Rennes, 10, 250 pp.

Marquer, D. 1989: Transfert de matière et déformation des granitoïdes. Aspects méthodologiques. Schweizerische Mineralogische und Petrographische Mitteilungen 69, 15–35.

Marquer, D. 1990: Structures et déformation alpine dans les granites hercyniens du massif du Gothard (Alpes centrales suisses). Eclogae Geologicae Helvetiae 83, 77–97.

Marquer, D. & Burkhard, M. 1992: Fluid circulation, progressive deformation and mass-transfer processes in the upper crust; the example of basement-cover relationships in the External Crystalline Massifs, Switzerland. Journal of Structural Geology 14, 1047–1057.

Marquer, D., Gapais, D. & Capdevila, R. 1985: Comportement chimique et orthogneissification d'une granodiorite en faciès schistes verts (Massif de l'Aar, Alpes Centrales). Bulletin de Minéralogie 108, 209–221.

Marquer, D. & Peucat, J.J. 1994: Rb-Sr systematics of recrystallized shear zones at the greenschist-amphibolite transition: examples from granites in the Swiss Central Alps. Schweizerische Mineralogische und Petrographische Mitteilungen 74, 343–358.

Maruyama, S., Suzuki, K. & Liou, J.G. 1983: Greenschist-amphibolite transition equilibria at low pressures. Journal of Petrology 24, 583–604.

Massonne, H.J. & Schreyer, W. 1987: Phengite geobarometry based on the limiting assemblage with K-feldspar, phlogopite, and quartz. Contributions to Mineralogy and Petrology 96, 212–224.

McCaig, A.M. 1997: The geochemistry of volatile fluid flow in shear zones In: Holness, M.B. (Ed), Deformation-Enhanced Fluid Transport in the Earth's Crust and Mantle, The Mineralogical Society series 8, 227–266.

Michalski, I. & Soom, M. 1990: The Alpine thermo-tectonic evolution of the Aar and Gotthard massifs, Central Switzerland: fission track ages on zircon and apatite and K-Ar mica ages. Schweizerische Mineralogische und Petrographische Mitteilungen 70, 373–387.

Milnes, A.G. 1976: Strukturelle Probleme im Bereich der Geotraverse: das Lukmanier-massiv. Schweizerische Mineralogische und Petrographische Mitteilungen 56, 615–618.

Milnes, A.G. & Pfiffner, O.A. 1980: Tectonic evolution of the Central Alps in the cross section St.Gallen-Como. Eclogae Geologicae Helvetiae 73, 619–633.

Mullis, J., Dubessy, J., Poty, B. & O'Neil, J. 1994: Fluid regimes during late stages of a continental collision: physical, chemical, and stable isotope measurements of fluid inclusions in fissure quartz from a geotraverse through the Central Alps, Switzerland. Geochimica et Cosmochimica Acta 58, 2239–2267.

Mullis, J. 1996: P-T-t path of quartz formation in extensional veins of the Central Alps. Schweizerische Mineralogische und Petrographische Mitteilungen 76, 159–164.

Müller, W., Mancktelow, N.S. & Meier, M. 2000: Rb-Sr microchrons of synkinematic mica in mylonites: an example from the DAV fault of the Eastern Alps. Earth and Planetary Science Letters 180, 385–397.

Müller, W., Prosser, G., Mancktelow, N.S., Villa, I.M., Kelley, S.P., Viola, G. & Oberli, F. 2001: Geochronological constraints on the evolution of the Periadriatic Fault System (Alps). International Journal of Earth Sciences 90, 623–653.

Müller, W., Kelley, S.P. & Villa, I.M. 2002: Dating fault-generated pseudotachylytes: Comparison of $^{40}Ar/^{39}Ar$ stepwise-heating, laser-ablation and Rb-Sr-microsampling analyses. Contributions to Mineralogy and Petrology 144, 57–77.

Pfiffner, O.A. 1986: Evolution of the north Alpine foreland basin in the Central Alps. In: Allen, P.A. & Homewood, P. (Eds.): Foreland Basins, Special Publications of the International Association of Sedimentologists 8, 219–228.

Pfiffner, O.A., Frei, W., Valasek, P., Staeuble, M., Levato, L., DuBois, L., Schmid, S.M. & Smithson, S.B. 1990a: Crustal shortening in the Alpine Orogen: results from deep seismic reflection profiling in the eastern Swiss Alps, Line NFP 20-East. Tectonics 9, 1327–1355.

Pfiffner, O.A., Klaper, E.M., Mayerat, A.M. & Heitzmann, P. 1990b: Structure of the basement-cover contact in the Swiss Alps. In: Roure, F., Heitzmann, P. & Polino, R. (Eds.): Deep Structure of the Alps, Société Géologique de France, Mémoire 156, 247–262.

Pfiffner, O.A. & Heitzmann, P. 1997: Geologic interpretation of the seismic profiles of the Central Traverse (lines C1, C2 and C3-north). In: Pfiffner, O.A., Lehner, P., Heitzmann, P., Mueller, St. & Steck, A. (Eds.): Deep Structure of the Swiss Alps: Results of NRP 20. Birkhäuser, Basel, Boston, Berlin, 115–122.

Philpotts, A.R. 1990: Principles of Igneous and Metamorphic petrology. Prentice Hall, Englewood Cliffs, NJ, United States, 498 pp.

Probst, P. 1980: Die Bündnerschiefer des nördlichen Penninikums zwischen Valser Tal und Passo di San Giacomo. Beiträge zur die Geologischen Karte der Schweiz, NF, 153.

Rahn, M.K., Brandon, M.T., Batt, G.E. & Garver, J.I. 2004: A zero-damage model for fission track annealing in zircon. American Mineralogist 89, 473–484.

Ruffini, R., Polino, R., Callegari, E., Hunziker, H. & Pfeiffer H. 1997: Volcanic clast-rich turbidites of the Tavayanne sandstones from the Thone syncline (Savoie France): records for a Tertiary post-collisional volcanism. Schweizerische Mineralogische und Petrographische Mitteilungen 77, 161–174.

Ruppel, C. & Hodges, K.V. 1994: Pressure-temperature-time paths from two-dimensional thermal models; prograde, retrograde, and inverted metamorphism. Tectonics 13, 17–44.

Ruppel, C., Royden, L. & Hodges, K.V. 1988: Thermal modeling of extensional tectonics; application to pressure-temperature-time histories of metamorphic rocks. Tectonics 7, 947–957.

Schaltegger, U. 1994: Unravelling the pre-Mesozoic history of Aar and Gotthard massifs (Central Alps) by isotopic dating: a review. Schweizerische Mineralogische und Petrographische Mitteilungen 74, 41–51.

Stalder, H.A. 1964: Petrographische und mineralogische Untersuchungen im Grimselgebiet (Mittleres Aarmassiv). Schweizerische Mineralogische und Petrographische Mitteilungen 44, 188–384.

Steck, A. 1966: Petrographische und tektonische Untersuchungen am zentralen Aaregranit und seinen altkristallinen Huellgesteinen im westlichen Aarmassiv im Gebiet Belalp-Grisighorn. Beiträge zur die Geolgischen Karte der Schweiz, NF, 130, 96 pp.

Steck, A. 1968: Die alpinischen Strukturen in den zentralen Aargraniten des westlichen Aarmassivs. Eclogae Geologicae Helvetiae 61, 19–48.

Steck, A. 1976: Albit-Oligoklas-Mineralgesellschaften der Peristeritluecke aus alpinmetamorphen Granitgneisen des Gotthardmassivs. Schweizerische Mineralogische und Petrographische Mitteilungen 56, 269–292.

Steck, A. 1984: Structures et déformations tertiaires dans les Alpes Centrales (transversale Aar-Simplon-Ossola). Eclogae Geologicae Helvetiae 77, 55–100.

Steck, A. & Burri, G. 1971: Chemismus und Paragenesen von Granaten aus Granitgneisen der Grünschiefer- und Amphibolitfazies der Zentralalpen. Schweizerische Mineralogische und Petrographische Mitteilungen 51, 534–538.

Steck, A. 1987: Le massif du Simplon – réflexions sur la cinématique des nappes de gneiss. Schweizerische Mineralogische und Petrographische Mitteilungen 67, 27–45.

Steck, A., Epard, J.L., Escher, A., Marchand, R., Masson, H. & Spring, L. 1989: Coupe tectonique horizontale des Alpes centrales. Mémoires de Géologie, Lausanne 5, 8.

Steck, A., Epard, J.L., Escher, A., Lehner, P., Marchant, R. & Masson, H. 1997: Geological interpretation of the seismic profiles through Western Switzerland: Rawil (W1), Val d'Anniviers (W2), Mattertal (W3), Zmutt-Findelen (W4) and Val de Bagnes (W5). In: Pfiffner, O.A., Lehner, P., Heitzmann, P., Mueller, S. & Steck, A. (Eds.): Deep structure of the Swiss Alps: Results of NRP 20 – Birkhäuser Verlag, Basel,123–137.

Steck, A., Epard, J.L., Escher, A., Gouffon, Y. & Masson, H. 2001: Carte géologique des Alpes de Suisse occidentale 1:100 000. Carte géologique spéciale N° 123, notice explicative. Office Fédéral des Eaux et de Géologie (Berne).

Stöckhert, B. & Gerya, T.V., 2005: Pre-collisional high pressure metamorphism and nappe tectonics at active continental margin: a numerical simulation. Terra Nova 17, 2, 102–110.

Villa, I.M. 1998: Isotopic closure. Terra Nova 10, 42–47.

Villa, I.M. & Puxeddu, M. 1994: Geochronology of the Larderello geothermal field: new data and the «closure temperature» issue. Contributions to Mineralogy and Petrology 115, 415–426.

Villa, I.M., Hermann, J., Müntener, O. & Trommsdorff, V. 2000: $^{39}Ar/^{40}Ar$ dating of multiply zoned amphibole generations (Malenco, Italian Alps). Contributions to Mineralogy and Petrology 140, 363–381.

Voll, G. 1976: Structural studies of the Valser Rhine Valley and Lukmanier region and their importance for the nappe structures of the Swiss Alps. Schweizerische Mineralogische und Petrographische Mitteilungen 56, 619–626.

von Raumer, J.F. 1984: The external massifs, relics of Variscan basement in the Alps. Geologische Rundschau 73, 1–31.

von Raumer, J.F., Abrecht, J., Bussy, F., Lombardo, B., Ménot, R.P. & Schaltegger, U. 1999: The Palaeozoic metamorphic evolution of the Alpine External Massifs. Schweizerische Mineralogische und Petrographische Mitteilungen 79, 5–22.

Wagner, G.A., Reimer, G.M. & Jaeger, E. 1977: Cooling ages derived by apatite fission-track, mica Rb-Sr and K-Ar dating. The uplift and cooling history of the Central Alps. Memorie degli Istituti di Geologia e Mineralogia dell' Universita di Padova 30, 1–27.

Yamada, K., Tagami, T. & Shimobayashi, N. 2003: Experimental study on hydrothermal annealing of fission tracks in zircon. Chemical Geology 201, 351–357.

Manuscript received July 10, 2007
Revision accepted November 27, 2007
Published Online first July 25, 2008
Editorial Handling: N. Macktelow, S. Bucher